separations

MDPI

Article

Enhanced Photocatalytic Activity of $CuWO_4$ Doped TiO_2 Photocatalyst Towards Carbamazepine Removal under UV Irradiation

Chukwuka Bethel Anucha [1,*], Ilknur Altin [1,*], Emin Bacaksız [2], Tayfur Kucukomeroglu [2], Masho Hilawie Belay [3] and Vassilis N. Stathopoulos [4]

1 Department of Chemistry, Faculty of Science, Karadeniz Technical University, Trabzon 61080, Turkey
2 Department of Physics, Faculty of Science, Karadeniz Technical University, Trabzon 61080, Turkey; eminb@ktu.edu.tr (E.B.); tayfun@ktu.edu.tr (T.K.)
3 Department of Science and Technological Innovation, University of Piemonte Orientale, Viale Teresa Michel 11, 15121 Alessandria, Italy; masho.belay@uniupo.it
4 Laboratory of Chemistry and Materials Technology, General (Core) Department, Psachna Campus, National and Kapodistrian University of Athens, 34400 Evia, Greece; vasta@uoa.gr
* Correspondence: C.B.Anucha@ktu.edu.tr (C.B.A.); ilknurtatlidil@ktu.edu.tr (I.A.)

Abstract: Abatement of contaminants of emerging concerns (CECs) in water sources has been widely studied employing TiO_2 based heterogeneous photocatalysis. However, low quantum energy yield among other limitations of titania has led to its modification with other semiconductor materials for improved photocatalytic activity. In this work, a 0.05 wt.% $CuWO_4$ over TiO_2 was prepared as a powder composite. Each component part synthesized via the sol-gel method for TiO_2, and $CuWO_4$ by co-precipitation assisted hydrothermal method from precursor salts, underwent gentle mechanical agitation. Homogenization of the nanopowder precursors was performed by zirconia ball milling for 2 h. The final material was obtained after annealing at 500 °C for 3.5 h. Structural and morphological characterization of the synthesized material has been achieved employing X-ray diffraction (XRD), Fourier transform infra-red (FTIR) spectroscopy, Brunauer–Emmett–Teller (BET) N_2 adsorption–desorption analysis, Scanning electron microscopy-coupled Energy dispersive X-ray spectroscopy (SEM-EDS), Transmission electron microscopy (TEM), X-ray photoelectron spectroscopy (XPS), and UV-Vis diffuse reflectance spectroscopy (UV-vis DRS) for optical characterization. The 0.05 wt.% $CuWO_4$-TiO_2 catalyst was investigated for its photocatalytic activity over carbamazepine (CBZ), achieving a degradation of almost 100% after 2 h irradiation. A comparison with pure TiO_2 prepared under those same conditions was made. The effect of pH, chemical scavengers, H_2O_2 as well as contaminant ion effects (anions, cations), and humic acid (HA) was investigated, and their related influences on the photocatalyst efficiency towards CBZ degradation highlighted accordingly.

Keywords: photocatalysis; $CuWO_4$-TiO_2; emerging contaminants; carbamazepine; water purification

Citation: Anucha, C.B.; Altin, I.; Bacaksız, E.; Kucukomeroglu, T.; Belay, M.H.; Stathopoulos, V.N. Enhanced Photocatalytic Activity of $CuWO_4$ Doped TiO_2 Photocatalyst Towards Carbamazepine Removal under UV Irradiation. *Separations* **2021**, *8*, 25. https://doi.org/10.3390/separations8030025

Academic Editor: Victoria Samanidou

Received: 31 December 2020
Accepted: 19 January 2021
Published: 26 February 2021

1. Introduction

Global technological advancement and improved human social welfare have led to the ubiquity of a group of synthetic and/or naturally occurring compounds not commonly monitored in the environment [1–3]. These compounds result in known or suspected adverse ecological and/or human health effects and have been identified and named emerging contaminants [2–4]. Release of contaminants of emerging concerns (CECs) and various other types of emerging organic contaminants (EOCs) have occurred steadily over a long time through several sources. However, more sophisticated detection and analytical technological techniques developed over the past decade had only made their recognition and detection possible with concentrations in the range of µg/L–ng/L [5,6]. Network of reference laboratories, research centers, and related organizations for the monitoring of emerging environmental substances (NORMAN) maintaining one of the

world's largest database records of CECs in the environment has over the last decade identified and listed over 1036 CEC compounds and their biotransformation products [7]. Among pharmaceuticals, Carbamazepine (CBZ), 5H-dibenzo[b,f]azepine-5-carboxamide, a dibenzoazepine derivative with structural similarity to tricyclic depressant used for the control of some type of seizures in the management of epileptic patients, has been classified by the NORMAN network as a psychoactive substance of pharmaceutical and personal care product (PCP) [8].

Due to little or near non removal of organic pollutants from wastewater treatment plants, technologies capable of handling these bio-recalcitrant compounds and dealing with their refractoriness have emerged [9]. Heterogeneous photocatalysis, an advanced oxidation process (AOP) technology, mainly based on TiO_2 semiconductor materials has been researched heavily with widespread dedicated attention due to its lifetime extension in resisting photochemical corrosion, non-toxicity, high photoreactivity, cost effectiveness, and biochemical inertness [9].

Low quantum efficiency of TiO_2 due to a faster recombination rate of valence band holes (h_{vb+}) and conduction band electrons (e_{cb-}) has been its setback. To this effect, research studies have been focused on improving the efficiency of TiO_2 based photocatalytic processes [9]. Doping, modification, semiconductor coupling, and sensitization with dyes could be regarded as popular strategies for the improvement of TiO_2 photocatalytic performance [10]. Among these strategies, a combination of two semiconductors with different energy band gaps (E_g) has proven to be efficient photo generators and improved photocatalytic activity [11]. Reports as well as comprehensive reviews on copper species modified TiO_2 photocatalysis have been published with majority of work focused on organic compound degradation, photocatalytic reduction reaction with hydrogen evolution, and/or CO_2 conversion to methane [12]. The Cu^{2+} ion-containing TiO_2 catalytic system makes it possible for TiO_2 to have faster consumption of (e_{cb-}) than O_2, which means that the rate of organic compound degradation may be higher. Furthermore, reduced Cu^{2+} ion (mainly Cu^+ ion) in the presence of O_2 in aqueous solution can easily be re-oxidized to Cu^{2+} ion on TiO_2 surface as the Cu^{2+}/Cu^+ redox recycle is easily facilitated [13]. Several research works have reported on the photodeposition of copper on titania surface as a means of Cu removal from water environment [14,15]. Over the last decade, it has been claimed that the binary catalyst system containing CuO and TiO_2 semiconductors increases photocatalytic activity [16]. Although CuO is highly effective in photocatalytic studies, it does not offer sufficient photocorrosion resistance and can leak Cu^{2+} ions into the environment and cause secondary pollution [9]. Therefore, there has been a great interest in both effective degradation of organic pollutants and the investigation of TiO_2 photocatalytic systems containing Cu species with high photostability [17].

As a dopant of TiO_2, $CuWO_4$ with ~2.2 eV band gap could be an alternative good candidate instead of CuO. $CuWO_4$ may have a faster and more effective driving force than CuO to scavenge (e_{cb-}) from TiO_2 due to its conduction band edge potential being more positive, which further enhances the performance of TiO_2 [18].

The synergistic effect of TiO_2-$CuWO_4$ composite on the degradation of atrazine, $CuWO_4$ modified TiO_2 nanoparticles on the degradation of eosin-Y, photocatalytic active ZnO/$CuWO_4$ nanocomposite on the decomposition of methylene blue (MO) and terephthalic acid (TPA) have all been studied [9,19,20]. Shia et al. investigated the photocatalytic activity of CuO photodeposited on TiO_2 for the degradation of 2,4-dichlorophenoxyacetic acid under UV irradiation [21]. CdS and $CuWO_4$ modified TiO_2 nanoparticles have been studied in comparison to TiO_2 with the former showing significant improvement under visible-light irradiation for the degradation of a dye (eosin-Y) and inactivation of a bacterium (Pseudomonas aeruginosa) [19]. Xiang et al. reported that the addition of $CuWO_4$ into the aqueous suspension of TiO_2 could result in significant enhancement in the rate of phenol degradation under UV light. They also reported that about 2.83 times more removal than the control was achieved with the $CuWO_4$ modified TiO_2 catalyst [17].

To the best of our knowledge, however, there are no reports on the application of $CuWO_4$-TiO_2 for the photocatalytic removal of CECs from water. This study, considered to be the first of its kind, reports promising results obtained over $CuWO_4$-TiO_2 composite catalyst prepared via a sol-gel process for the TiO_2 content and hydrothermal assisted co-precipitation for the $CuWO_4$ phase. A 0.05 wt.% $CuWO_4$ over TiO_2, composite was applied for carbamazepine degradation under near visible light. In addition, influences of various experimental parameters such as pH, H_2O_2, contaminant ions (cations and anions), and humic acid on photocatalytic degradation were also investigated. Moreover, major oxidizing species for CBZ degradation were also investigated.

2. Materials and Methods

2.1. Chemicals

Titanium isopropoxide (TiP), ethanol, hydrochloric acid, copper nitrate dihydrate (>98%), sodium tungstate dihydrate (>99%), carbamazepine (>99%), Na_2SO_4, $NaNO_3$, Na_2CO_3, $NaHCO_3$, NaCl, NaF, Na_2HPO_4, $CaCO_3$, $MgCO_3$, K_2CO_3, NH_4Cl, and sodium humic acid salt were purchased from Sigma Aldrich (Darmstadt, Germany). All chemicals were of analytical grade and employed as purchased without further purification. Milli-Q water was used throughout the entire experiment for the photocatalytic studies.

2.2. Preparation of Catalyst ($CuWO_4$-TiO_2)

Initially, the sol-gel method was employed for the synthesis of TiO_2 [22,23]. Briefly, 7.9 mL of titanium isopropoxide, used as a precursor of TiO_2, was introduced into 150 mL of ethanol in a glass flask. Keeping the mixture under stirring, 0.5 mL of distilled water, and 220 µL of 12 M HCl were added sequentially and the suspension stirred for 8 h. The formed gel was then dried at 80 °C for 12 h. This precursor was used for the preparation of composites $CuWO_4$-TiO_2 as described below and to obtain also the unmodified TiO_2 powder after calcination at 600 °C for 2 h.

$CuWO_4$ powder was prepared by the co-precipitation assisted hydrothermal method from hydrated salts of $Cu(NO_3)_2{\cdot}2H_2O$, and $Na_2WO_4{\cdot}2H_2O$ as precursors; with equimolar quantities of these salts dissolved separately in distilled water of volume 25 mL [24]. Sodium tungstate dihydrate as solution A was dropwise added to copper nitrate dihydrate solution B under continuous stirring. Solution mixture was stirred for 15 min followed by heating for 3 h at 85 °C. Obtained precipitates were collected, washed thoroughly with distilled water, and dried at 90 °C overnight and subsequently calcined at 500 °C for 3.5 h to obtain $CuWO_4$ powder.

Finally, the obtained TiO_2 precursor and different amounts of $CuWO_4$ precursor were mixed to form (0.05, 1, 2, 3, and 4 wt.% in TiO_2, respectively. The final composites were prepared after ball milling using zirconia balls for 2 h and calcination at 500 °C for 3 h. Following preliminary photocatalytic tests, 0.05 wt.% $CuWO_4$-TiO_2 (0.05$CuWO_4$-TiO_2) was selected as the best performing material from the 0.05, 1, 2, 3, and 4 wt.% $CuWO_4$ in TiO_2 series. In addition, 0.05$CuWO_4$-TiO_2 was employed throughout the experiments both for structural characterization and catalytic performance properties.

2.3. Characterization of Catalysts

X-ray diffraction (XRD) measurement was carried out using a Rigaku D/Max-IIIC diffractometer (RIGAKU Corp; Tokyo, Japan) with CuKα radiation (λ = 0.1541 nm) over the range 2θ = 10–70° at room temperature, operated at 35 kV and 25 mA at the rate of 3°/min scan speed [25–27]. Fourier transform infrared (FTIR) spectroscopy was performed on a PerkinElmer FT-IR spectrometer (Thermo Fisher Scientific, Leicestershire, UK) employing attenuated total reflection (ATR) method. A Brunauer–Emmett–Teller (BET) technique was recorded on the nitrogen adsorption–desorption at 76 K using a Micromeritics 3 Flex version 5.00 (Micromeritics, Norcross, GA, USA) after degassing [25–27]. Morphology of the synthesized materials was determined with scanning electron microscopy (SEM) ZEISS EVO LS10 (Carl Zeiss Microscopy, Hamburg, Germany), of 0.2–30 kV acceleration voltage

and 0.5 pA–5 μA probe current, coupled to energy dispersive spectroscopy (EDS) detector (Carl Zeiss SmartEDX, Hamburg, Germany), with samples attached to sample holder and coated with gold using sputter-coating (SEM Coating System Machine). Transmission electron microscopy (TEM) was performed by FEITecnaiG2 Spirit (FEI, Hillsboro, OR, USA). X-ray photoelectron spectroscopy (XPS) measurement was carried out using a PHI 5000 VersaProbe spectrometer (ULVAC PHI, Inc., Kanagawa, Japan) with an AlKα radiation source. Optical properties of the materials were obtained with UV-Vis diffuse reflectance spectroscopy (UV-Vis DRS) in absolute measurement using $BaSO_4$ reference plate [25–27].

2.4. Photocatalytic Experiments

The photocatalytic performance of the synthesized $CuWO_4$-TiO_2 materials was evaluated towards the degradation of carbamazepine under near visible light (λ = 365 nm). A Five 100 W ultraviolet Philips Mercury (Hg) lamp (TL-K 40W/10R ACTINIC BL REFLECTOR, Hamburg, Germany) of intensity 1.2 mW/cm^2 was used as the irradiation light source [2]. In addition, 40 mL of working suspension containing 1 g/L of catalyst and 10 mg/L CBZ were introduced into 50 mL capacity cylindrically shaped quartz glass sleeve reactor cells and kept under agitation during irradiation. Prior to irradiation, the suspension was stirred in the dark for 30 min to establish adsorption–desorption equilibrium while at the same time irradiation stability was achieved. Employing HANNA, edge pH Meter (Woonsocket, RI, USA), pH values of 3, 5, 9, and 11 were controlled and tested during photocatalytic experimental runs and finally experiments were carried out at around pH 8 close to the initial natural pH 7.78 of working suspension. All other conditions of 40 mL working suspension volume, 1 g/L of catalysts amount, 10 mg/L CBZ concentration, irradiation time of 4 h, and 30 cm sample to light source distance have remained constant throughout the experiment unless otherwise stated. At given time intervals, 1 mL sample aliquots were drawn from the reactor cells and filtered through the membrane filter (0.45 μm) and analyzed by HPLC for monitoring the degradation of CBZ, using an Inertsil ODS-3 C18 column (5 μm, 4.6 mm × 150 mm) purchased from GL Sciences Inc. (Tokyo, Japan). Retention time was 6 min, and the eluent was a mixture of 35% phosphoric acid in water (pH ~3) and 65% acetonitrile with a flow rate of 1 mL/min. CBZ concentrations were evaluated at 285 nm wavelength. Besides the photocatalyst activity monitoring, experiments of photolysis without catalysts as well as heat effect with and without catalyst towards the degradation of the organic substrate by wrapping the reactor cells with aluminum foils to help protect irradiated samples from light interference were also carried out. All photocatalytic experimental data were the average value of triplicate measurements.

Evaluation of kinetic rate constant was monitored as investigational value for the remaining CBZ concentration over irradiation time window of 2 h exposure, and data were fixed by the pseudo-first order model using the rate equation:

$$-\ln C/C_0 = k_{app}t \quad (1)$$

where, k_{app}, C_0, and C are apparent degradation rate constant, initial concentration, and concentration after time t, respectively.

3. Results and Discussion

3.1. Characterization of Catalysts

Figure 1A depicts the XRD pattern of synthesized TiO_2, $CuWO_4$, and 0.05$CuWO_4$-TiO_2. It has been reported in previous studies that the diffraction intensity of $CuWO_4$ reaches a maximum at 500 °C calcination temperature [9]. From Figure 1A, a triclinic structure was observed for $CuWO_4$ calcined at 500 °C and confirmed with JCPDS Card No. 01-073-1823 [28]. A typical anatase pattern of pure TiO_2 was identified with characteristic peaks at 25.3°, 36.9°, 37.8°, 38.7°, 48.1°, 53.9°, 55.1°, 62.7°, and 68.8° corresponding to the (101), (103), (004), (112), (200), (105), (211), (204), and (116) crystal planes (JCPDS Card No. 01-071-1168). In the XRD pattern of the 0.05$CuWO_4$-TiO_2, the anatase peaks of

TiO_2 are identified (Figure 1A). As can be seen again, from Figure 1A, incorporation of $CuWO_4$ onto the TiO_2 has not changed the crystalline phase of the as prepared anatase TiO_2. No new crystal phases are observed, and no solid state reactions exist. Small peaks corresponding to $CuWO_4$ are recorded due to the low loading percentage [29–31]. Crystal size of TiO_2 in the $0.05CuWO_4$-TiO_2 showed a slight increase over unmodified TiO_2 as depicted in Table 1. This may be attributed to the additional processing via ball milling and annealing of the composite. The crystal size (d_{XRD}) of the materials has been estimated using the Debye Scherrer function as given below:

$$d_{XRD} = K\lambda/(\beta Cos\theta) \quad (2)$$

where $\lambda = 0.1541$ nm is the wavelength of the CuKα source, β is the line width at half maximum height, K is the shape factor kept at constant value of 0.89, and θ is the diffraction angle.

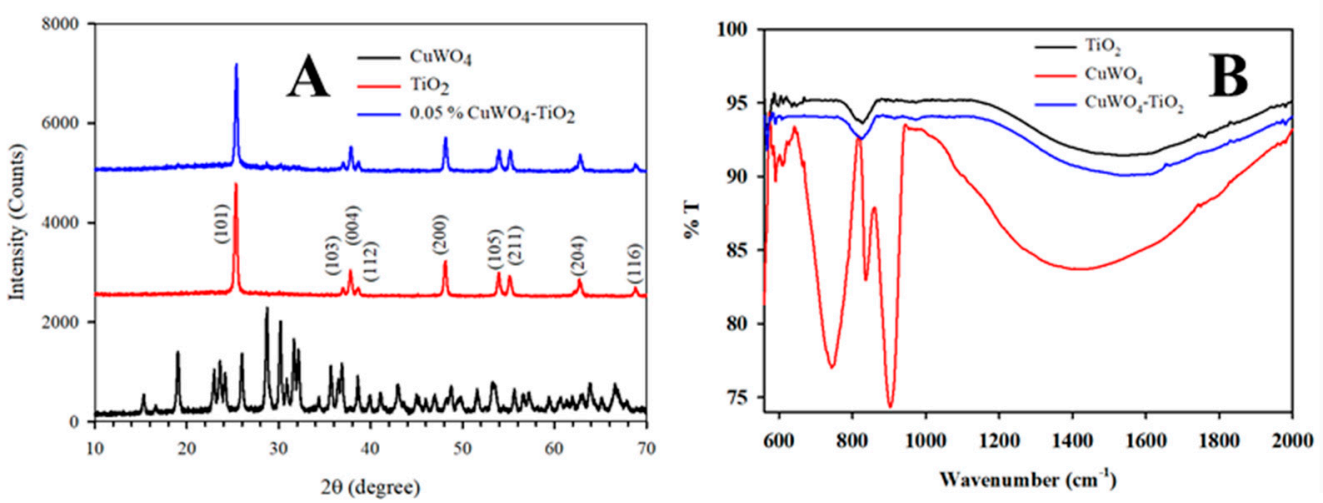

Figure 1. (**A**) XRD pattern and (**B**) FTIR spectra of as synthesized materials.

Table 1. Morphological and structural characteristics of synthesized materials [a].

Materials	d_{XRD} (nm)	d_{TEM} (nm)	S_{BET} (m^2/g)	V_p (cm^3/g)	d_p (nm)	E_g (eV)
TiO_2	26.5	35.3	4.7	0.0047	5.6	3.2
$0.05CuWO_4$-TiO_2	28.0	36.3	2.3	0.0032	6.0	2.7

[a] d_{XRD}, crystallite size estimated by XRD; d_{TEM}, particle size estimated by TEM; S_{BET}, surface area; V_p, total pore volume; d_p, average pore size; E_g, energy band gap.

FTIR spectra of TiO_2 and its $CuWO_4$ modified form (Figure 1B) indicate that the introduction of $CuWO_4$ did not alter the spectra of pure TiO_2, as evidenced by the presence of stretching HOH signal of water molecules at around 1600 cm^{-1} [32]. However, the stretching vibrational signal of the other hydroxyl groups (-OH) between 3100–3750 cm^{-1} remains absent in obtained material spectra due to the small surface area of synthesized materials (Table 1), which made it impossible to affiliate -OH functional group of surface adsorbed water molecules within this range. The characteristic Ti-O stretching and Ti-O-Ti linkages in titania nanoparticles were evident in both samples of pure TiO_2 and $0.05CuWO_4$-TiO_2 at around the 800 cm^{-1} region [32]. Characteristic bands of $CuWO_4$ occurring at around 550 cm^{-1}, 790 cm^{-1}, and 800 cm^{-1}–900 cm^{-1} for Cu-O stretching vibrations, Cu^{n+}-O^{2-}-W^{n+} vibration respectively as well as the stretching O-H vibration at around 1400 cm^{-1} confirm successful synthesized $CuWO_4$ [24,32].

The N_2 adsorption–desorption isotherm of synthesized materials in Figure 2A corresponds to low surface area of materials for both cases. Minor hysteresis indicates the existence of few mesopores [31,33]. The BJH pore size distributions (PSD) shown in Figure 2B with pore size maxima higher than 3 nm reveal the available mesopores that can further be supported by type IV adsorption–desorption isotherms (Figure 2A). The porosity data are reported in Table 1. The surface area (S_{BET}), of 0.05$CuWO_4$-TiO_2 decreased with respect to TiO_2 due to the addition of $CuWO_4$ [26].

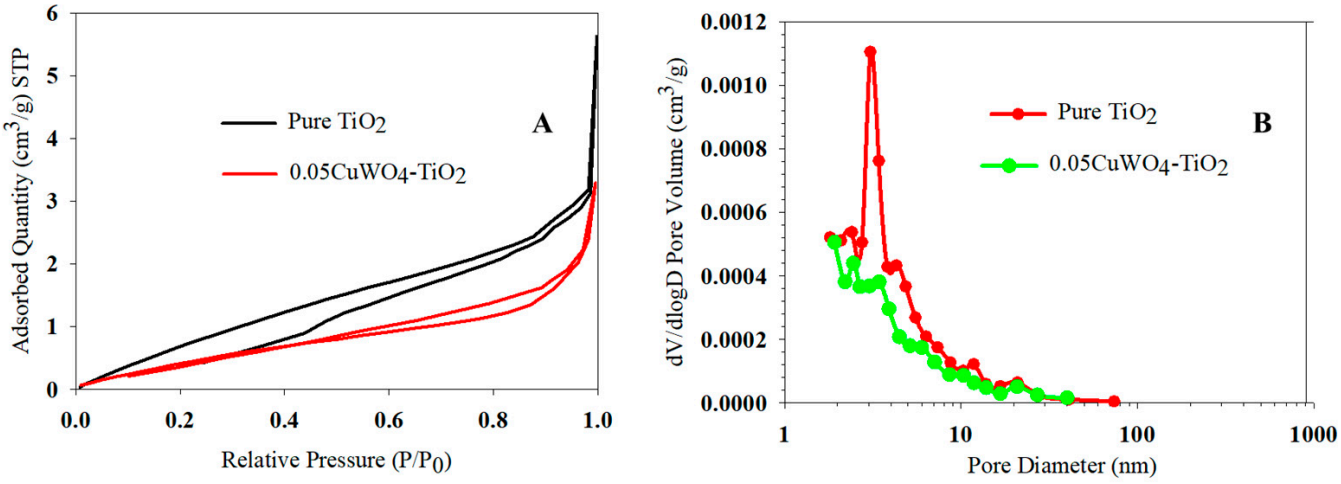

Figure 2. (**A**) N_2 adsorption–desorption isotherm, and (**B**) BJH pore size distribution of synthesized materials.

The morphology of the prepared TiO_2 can be seen in the SEM images (Figure 3A). Particles of plate-like shape with irregular edges are observed. The respective particles of $CuWO_4$ (Figure 3B) show a more irregular structure. The obtained 0.05$CuWO_4$-TiO_2 composite looks more like the TiO_2 plate-like particles. $CuWO_4$ particles are identified finely deposited on the surface of the TiO_2 plates in Figure 3C. The uniform distribution of $CuWO_4$ is confirmed by the energy dispersive X-ray Spectroscopy (EDS) spectra map. The elemental composition of the sample materials expressed in weight and atomic percentages agreed approximately with their respective stoichiometric proportions. The Au element presence in the EDS map of Figure 3B,C is of the gold coated origin during sample preparation.

TEM reveals the details of interaction of $CuWO_4$ and TiO_2. The primary particle size has increased after the addition of $CuWO_4$. Figure 4A,B reveal the isolated nature of TiO_2 particles that appear more agglomerated upon the addition of $CuWO_4$ onto TiO_2. This feature is in line with the observed decrease in specific surface area value (Table 1). The particle size of the materials as revealed by TEM measurements was obtained using ImageJ Software (Version 1.41) and is reported in Table 1. A very small increase of particle size of 0.05$CuWO_4$-TiO_2 material is found at 36.3 nm compared to that of unmodified TiO_2 at 35.3 nm. This result is in agreement with the average crystallite size by XRD, where, again, 0.05$CuWO_4$-TiO_2 showed a slightly larger crystal size over unmodified TiO_2. However, due to the polycrystalline nature of titania, a direct relation among the methods is not favored.

As shown in Figure 5A,a–f, the chemical environment of pure TiO_2 and 0.05$CuWO_4$-TiO_2 materials, and their associated chemical states is depicted. The XPS survey spectrum of 0.05$CuWO_4$-TiO_2 material contain, in addition to Ti, O elements derived from the TiO_2 portion of the composite; W and Cu and indicate the presence of $CuWO_4$ in the composite (Figure 5A) [31]. As can be seen from Figure 5a, two peaks of W 4f resolved at 35.3 eV and 36.7 eV corresponding to the deconvoluted binding energies of $W4f_{5/2}$ and $W4f_{7/2}$ respectively were observed in the 0.05$CuWO_4$-TiO_2 sample material. The possible generation of Ti^{3+} by Ti^{4+} via electron transfer from the conduction band of TiO_2 to the deep-lying conduction band of WO_3, where the reduction of W^{6+} could occur to form W^{5+}

with accompanied re-oxidation of the Ti^{3+} species to form Ti^{4+} during redox mechanism, is envisaged; as +6 oxidation state of W in metal tungstates has been reported [30,34,35]. Hence, in the XPS spectral data, there has not been a fitting for Ti^{3+} [30]. The consequent effect of this could be seen in the improved photocatalytic properties of the composite. In agreement with reported data, the binding energy of resolved deconvoluted Ti 2p of the pure TiO_2 component of the 0.05$CuWO_4$-TiO_2 (red line) and that of pure unmodified TiO_2 (black line) were obtained and attributed to Ti^{4+} at 458.7 eV and 458.1 eV binding energies for Ti $2p_{3/2}$ and 464.5 eV, and 463.7 eV binding energies for Ti $2p_{1/2}$, respectively, as can be seen in Figure 5b,e [29,30,36–38]. From Figure 5c, a deconvoluted Cu 2p spectrum of $2p_{3/2}$ was obtained at binding energy of 934.9 eV and was in the range of values already reported in literature attributed to Cu^{2+} states [9,34,37–41]. Figure 5d,f showed binding energy of O 1s of 0.05$CuWO_4$-TiO_2 at 528.9 eV, reported to be accounted for adsorbed hydroxyl or oxygen molecule [38], while that of TiO_2 at 529.9 eV comes possibly from the crystal lattice oxygen (O-Ti^{4+}) in the TiO_2. The 0.05$CuWO_4$-TiO_2 composite material depicted approximately the same binding energies between its Ti 2p and O 1s spectra of the synthesized materials. However, a shift in peak of about 0.6 eV and 0.8 eV for pure TiO_2 in relation to 0.05$CuWO_4$-TiO_2 at respective BEs (458.7 eV, 458.1 eV) for Ti $2p_{3/2}$, and (464.5 eV, 463.7 eV) for Ti $2p_{1/2}$ ascribed to each of the two materials was observed, as can be seen from Figure 5b,e. A similar observation can be seen in Figure 5d,f of O 1s, where a shift of about 1.0 eV occurred between TiO_2 at 529.9 eV BE and that of 0.05$CuWO_4$-TiO_2 at 528.9 eV BE. These shifts have been attributed to the modification of TiO_2 by $CuWO_4$ [42,43].

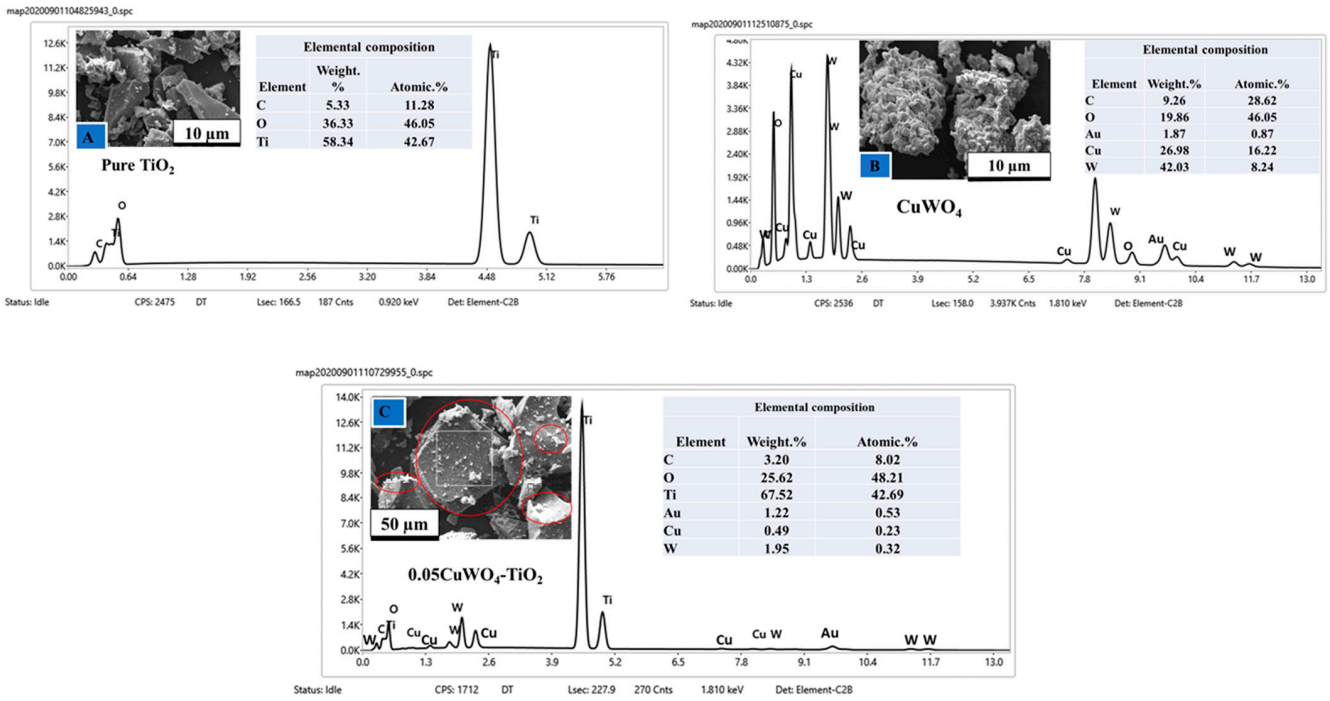

Figure 3. SEM images and corresponding EDS map of (**A**) TiO_2, (**B**) $CuWO_4$, and (**C**) 0.05$CuWO_4$-TiO_2.

Energy band gaps of TiO_2 and 0.05$CuWO_4$-TiO_2 photocatalyst materials were evaluated using Equation (3) of Kubelka–Munk [44] and shown in Figure 6:

$$(\alpha h\nu) = A(h\nu - E_g)^n \quad (3)$$

Expressing the parametric functions of Equation (3), α represents semiconductor optical absorption coefficient, $h\nu$; the energy of incident photons, A; constant, E_g; the band gap energy and n; the number of transitions, taken as 1/2 for indirect energy band gap estimation.

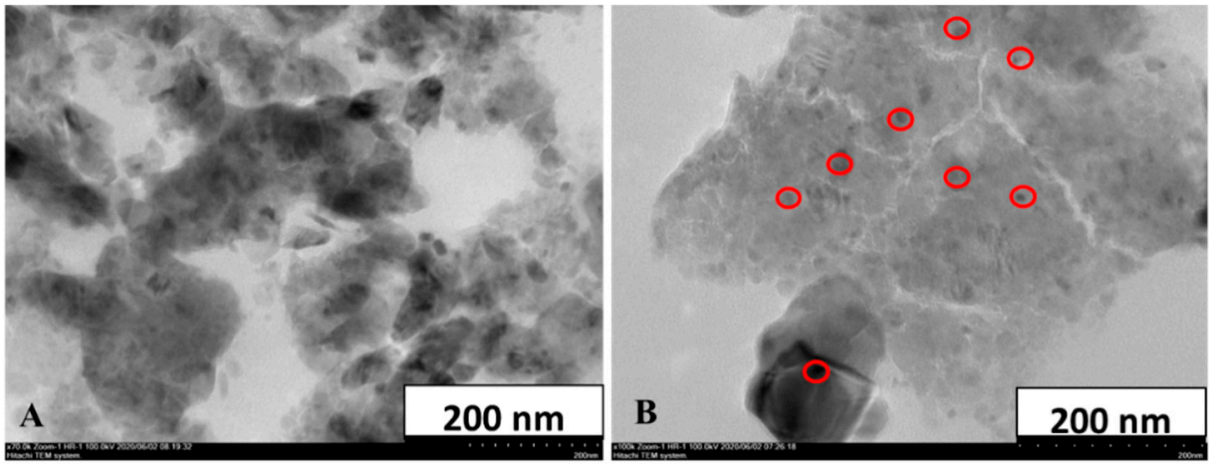

Figure 4. TEM micrographs of (**A**) TiO_2, and (**B**) $0.05CuWO_4$-TiO_2.

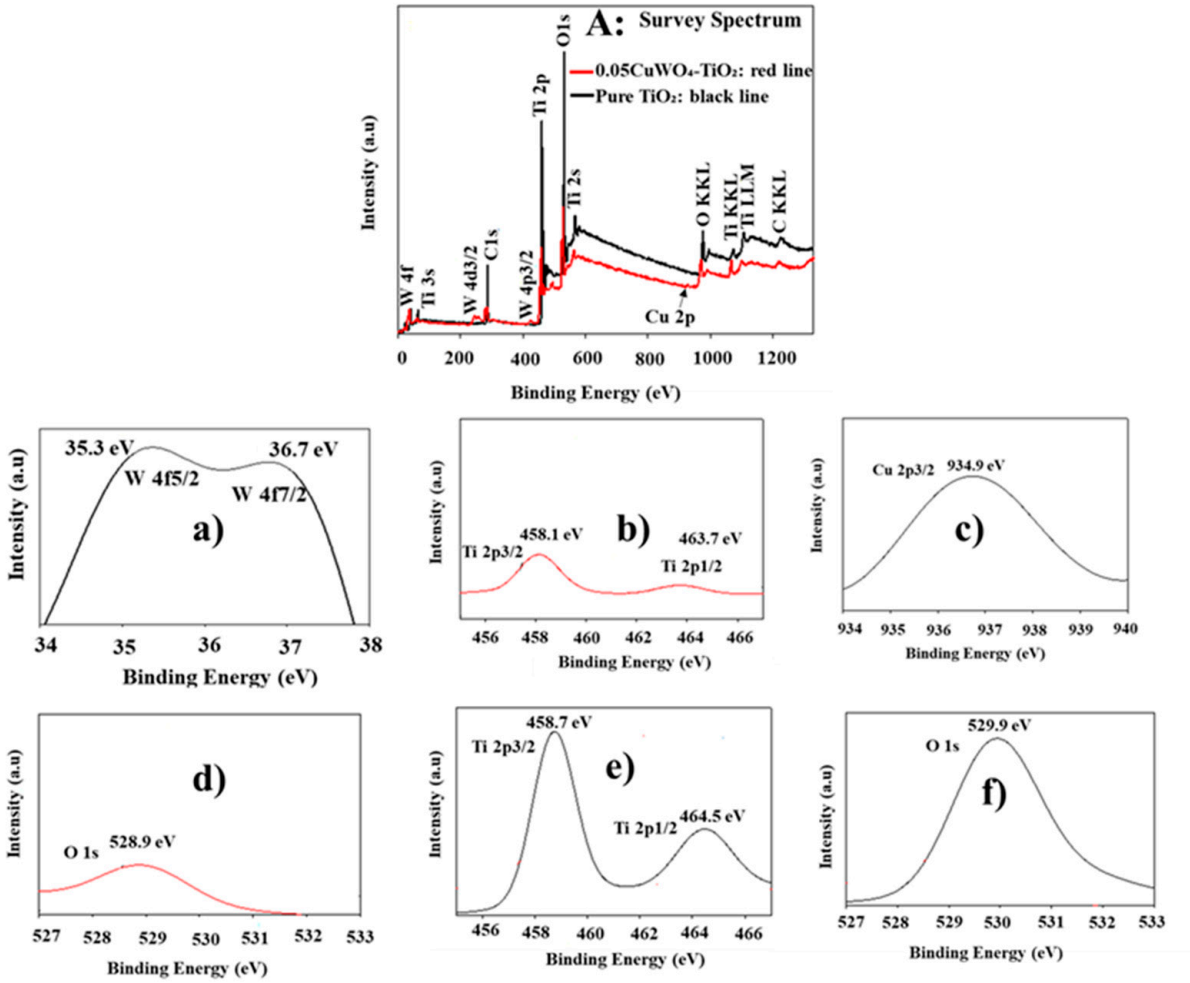

Figure 5. XPS measurement of sample materials: (**A**) Survey spectrum of pure TiO_2 (black line) and $0.05CuWO_4$-TiO_2 (red line) differentiating common elements of both materials and, their corresponding deconvoluted spectra of (**a**) W 4f; (**b**) Ti 2p (red line); (**c**) Cu 2p; (**d**) O 1s (red line); (**e**) Ti 2p (black line), and (**f**) O 1s (black line).

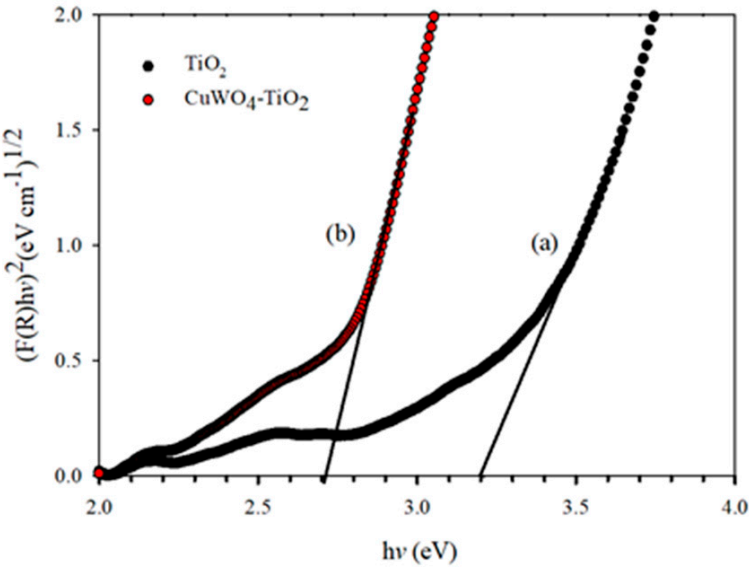

Figure 6. Energy band gap measurement of (**a**) TiO_2 (black line), and (**b**) $0.05CuWO_4$-TiO_2 (red line).

Energy band gap (E_g) values of 2.7 eV and 3.2 eV were obtained for $CuWO_4$-TiO_2 and TiO_2, respectively, by the intercept of the extrapolated straight line to the energy axis $(\alpha h\nu)^2$ curves of the photocatalysts materials as depicted in (Figure 6, Table 1). Obtained values agree with previously reported energy band gap values of TiO_2 and its Cu modified forms [19]. The energy band gap of $CuWO_4$, which displays an indirect electronic transition and haven been reported at values between 1.9 eV to 2.45 eV [9,28,29,45], is not far from the obtained value of 2.7 eV for $CuWO_4$ modified TiO_2 material reported herein. However, such a E_g value of $CuWO_4$-TiO_2 material indicates a successful modification approach for the $CuWO_4$-TiO_2 sample via the octahedral CuO_6 cluster distortion in the $CuWO_4$ material [39,46].

3.2. Photocatalytic Activity

The photocatalytic efficiency of the prepared 0.05, 1, 2, 3, and 4 wt.% $CuWO_4$ in TiO_2 series samples noted as $0.05CuWO_4$-TiO_2, $1CuWO_4$-TiO_2, $2CuWO_4$-TiO_2, $3CuWO_4$-TiO_2, and $4CuWO_4$-TiO_2, respectively, was evaluated towards CBZ under near visible light wavelength of 365 nm for irradiation exposure time of 4 h (Figure 7). A comparison to TiO_2 and $CuWO_4$ control samples was also made. In addition, a $0.05CuWO_4$-TiO_2 photocatalyst degraded almost completely the CBZ within 2 h irradiation exposure. On the contrary, the TiO_2 sample achieved around 85% CBZ degradation while the pure $CuWO_4$ material did not show any CBZ degradation throughout the 4 h irradiation exposure time. As can be seen, the photocatalytic activity of $CuWO_4$-doped TiO_2 decreased with an increase in loading amount of $CuWO_4$ from 0.05 wt.% to 4 wt.% (Figure 7a) following a CBZ removal trend of $0.05CuWO_4$-TiO_2 > $1CuWO_4$-TiO_2 > $2CuWO_4$-TiO_2 > $3CuWO_4$-TiO_2 ~ = $4CuWO_4$-TiO_2. Generally, the observed trend of decrease in photocatalytic activity with increase in weight percentage load of $CuWO_4$ can be attributed to the absorption of incident light by the excess $CuWO_4$, thereby reducing the number of photons reaching the TiO_2, particle agglomeration leading to active site blockage, effects of dissolved cupric species, and possibility of charge transfer from composite to O_2 or target molecules during photocatalysis [9,17,20,30,40,47,48], hence, why the minute added $0.05CuWO_4$ onto TiO_2 produced a better photocatalytic activity in the series. From Figure 7b, apparent degradation rate constants of the photocatalyst materials were recorded highest for the $0.05CuWO_4$ modified TiO_2 material at ~2 h^{-1} compared to 0.89 h^{-1} for TiO_2 and negligible for $CuWO_4$ material due to lack of photocatalytic activity during 4 h irradiation time. The photocatalytic degradation followed pseudo-first-order kinetics as can be seen from the fitted apparent rate degradation constant curve of Figure 7b [17,20]. In the absence of the photocatalyst

and under light irradiation alone, (Figure 7c), about 20% CBZ was degraded during 4 h irradiation. Other influences like dark test and heat effect with and without catalyst during the 4 h irradiation time, as can be seen from Figure 7c, were investigated showing insignificant CBZ degradation. The overall CBZ degradation rate of $0.05CuWO_4$-TiO_2 was ~2 times higher than that of TiO_2 at 2 h of the 4 h irradiation exposure window. This was an impressive improvement of the photocatalytic activity in $CuWO_4$-TiO_2 nanocomposite material by the synergistic effect of the introduction of $CuWO_4$ over TiO_2 [9,17,48].

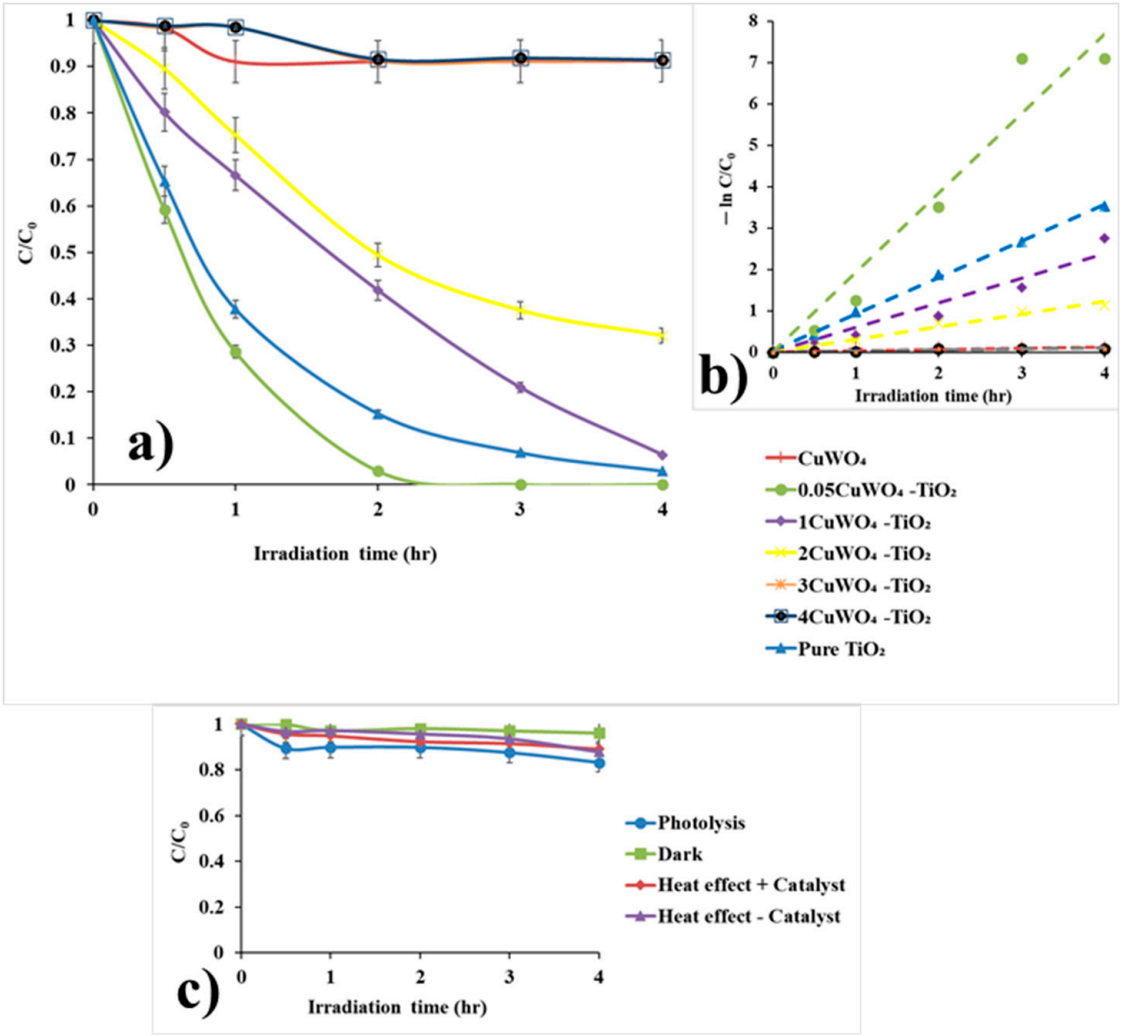

Figure 7. Photocatalytic degradation of CBZ by (**a**) 0.05, 1, 2, 3 and 4 wt.% $CuWO_4$ in TiO_2 series (C_0 = 10 mg/L, catalyst dosage = 1.0 g/L, pH 7.78), and (**b**) the corresponding degradation rate kinetics plot, and (**c**) photolysis, dark tests, and effects of heat with and without catalyst.

3.2.1. Effect of pH

As an important parameter in photocatalytic reactions, pH influences surface charge properties of photocatalyst materials and have triggered efforts in trying to understand its role along or in combination with other significant features in photocatalysis such as semiconductor surfaces, solvent molecule, and substrate properties [49,50]. To assess the effect of the initial pH on the photocatalytic degradation of CBZ, different pH values in the range from 3 to 11 were tested in the presence of 1 g/L $0.05CuWO_4$-TiO_2. As illustrated in Figure 8, $0.05CuWO_4$-TiO_2 photocatalyst delivered almost a 100% CBZ degradation after 2 h irradiation exposure at natural pH 7.78; other pH values of 3, 5, 9, and 11 were also investigated for their influence on the degradation ability of the material. $0.05CuWO_4$-TiO_2

nanocomposite exhibits a higher efficiency in the photocatalytic degradation process at pH 3 most probably due to high H^+ concentrations. The formation of hydroperoxide radical ($HO_2^{\bullet}$) and hydrogen peroxide (H_2O_2), both important reactive species in photocatalytic degradation, have been reported in acidic conditions and are responsible for such a catalytic behavior [51,52]. At such a low pH = 3, CBZ degradation efficiency was slightly improved over what was achieved under the initial natural pH condition of around 7.78 (Figure 8). As can be seen from Figure 9, the photocatalytic degradation of CBZ over pure $CuWO_4$ was also evaluated at pH 3–11. No significant activity was observed even after 4 h irradiation. Such reported photostability of $CuWO_4$ could possibly also have impacted the insignificant activity observed in the tested pH conditions [17]. Since $CuWO_4$ degradation activity over CBZ is not affected by pH (Figure 9) in contrast to 0.05$CuWO_4$-TiO_2 material, it is expected that the point of zero charge (pH_{pzc}), which, in general, is crucial for heterogeneous photocatalytic systems, was reliant on the TiO_2 phase.

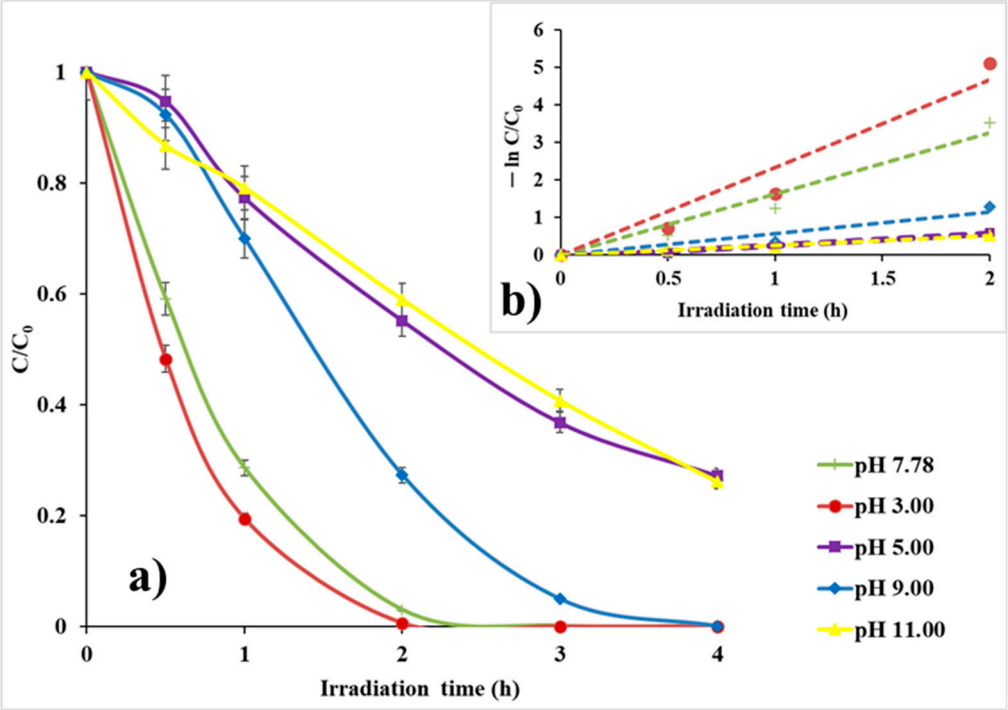

Figure 8. (**a**) Effect of initial pH on CBZ degradation by 0.05$CuWO_4$-TiO_2 (C_0 = 10 mg/L and catalyst dosage = 1.0 g/L), and (**b**) the apparent degradation rate constants (inset).

TiO_2 based photocatalysts have pH_{pzc} in the range of 5.5–6.5 [53] and, therefore, under our initial pH working condition, the surface of the catalyst will be partially protonated. Consequently, undissociated CBZ and its ions in protonated and deprotonated forms will be present under this condition and, therefore, attracted to the surface of the catalyst by electrostatic forces and eventually degrade. The comparable degradation activity at pH 3 is due to the enhanced acidic proton environment facilitating the generation of more reactive species ($HO_2^{\bullet}$, H_2O_2) that promotes the photodegradation process. However, at pH 5, the surface of TiO_2 phase of the composite is nearly neutral according to the pH_{pzc} value, and therefore will attain no net charge with respect to the catalyst surface for subsequent degradation, thereby presenting more CBZ in aqueous solution [49,50,53], shielding, and hindering light penetration for improved photo activity. At pH = 9, a considerate degradation rate of CBZ by the photocatalyst material was observed as well and at 4 h irradiation. Over 90% CBZ degradation was observed in comparison to its initial concentration in the photocatalytic system. On the other hand, at pH = 11, low degradation of CBZ over the 4 h irradiation was observed. The implication of this is that with the investigated catalyst,

moderate acidic pH = 5 and advanced pH = 11 values did not favor CBZ removal during 4 h irradiation time, as compared to almost neutral pH = 7.78 (the initial unmodified working suspension pH), moderate pH = 9 and lower acidic pH = 3. The reason for low CBZ removal at higher alkaline pH = 11 has been reported as a result of the inhibitory catalyst effect as the CBZ ionic form becomes more stabilized and tends to molecular form in aqueous solutions at such an advanced pH value [6]. The tested pH range ($3 \leq pH \leq 11$) in this study was set to cover most wastewaters and natural waters. Although the best pH value (7.78) was identified, discrepancies rather than a clear trend were found in the efficiency of the catalyst performance over pH on the degradation of CBZ. CBZ and other organic pollutants photocatalytic degradation processes have been reported to be influenced by the derivatives from parent molecules [54]. In order to gather more information on the photocatalytic performance of $0.05CuWO_4$-TiO_2 over CBZ, further tests were conducted under the best performing pH conditions as described next.

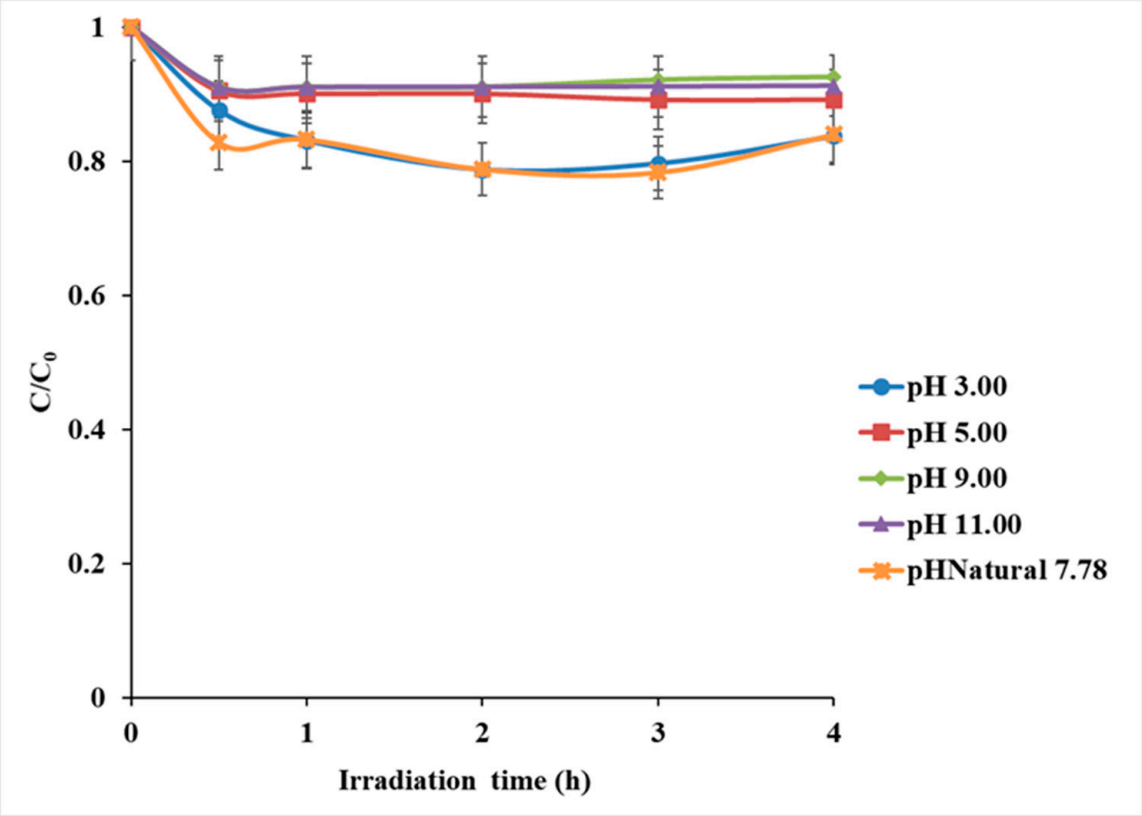

Figure 9. Effect of initial pH on CBZ degradation by $CuWO_4$ (C_0 = 10 mg/L and catalyst dosage = 1.0 g/L).

3.2.2. Effect of Chemical Scavengers

To probe reactive oxygen species (ROS) during the degradation process, trapping tests were carried out on the $0.05CuWO_4$-TiO_2 catalyst under experimental conditions of C_0 = 10 mg/L, catalyst dosage = 1.0 g/L, pH 8 (Figure 10). Solutions of 1 mM each of benzoquinone (BQ, a $O_2^{\bullet -}$ radical scavenger), isopropyl alcohol (IPA, a $^{\bullet}OH$ radical scavenger), ethylenediamine tetra acetic acid (EDTA, a h^+ scavenger) and sodium sulphate (Na_2SO_4, an e^- scavenger) recognized as ROS quencher chemicals were added to the working suspension and consequent quenching effects monitored accordingly [55]. Electrons that were able to move from the conduction band of TiO_2 to the conduction band of $CuWO_4$ as well as the valence band holes of $CuWO_4$ may not have been all directly involved in the photocatalytic degradation of CBZ but may be responsible for the formation of possible Cu^{2+}/Cu^+ and W^{6+}/W^{5+} redox pairs. Subsequent reformations involving holes can gener-

ate reactive species responsible for degradation. For the case of probing for valence band hole (h^+) effect on the degradation process, the apparent rate degradation constant reduced to about ~5.5 times in comparison to no scavenger addition. CBZ degradation of about 65% was achieved after 4 h irradiation in the presence of hole scavenger. With the introduction of BQ, to probe superoxide anion ($O_2^{\bullet-}$) effect on the degradation process, the reduction of the degradation rate constant was about ~5.9 times compared to when no scavenger was added. In this case, CBZ degradation was suppressed to 60% in 4 h of irradiation. For the effects of hydroxyl ($^{\bullet}OH$) species on the degradation process, the introduction of IPA led to photodegradation rate constant reduction of about 8 times, with CBZ degradation reaching just over 60% after 4 h irradiation. According to these results, it can be deduced that basic reactive oxygen species of superoxide anion ($O_2^{\bullet-}$) and hydroxyl ($^{\bullet}OH$) radical species generated via hole charge carriers as key drivers were primarily involved in the photocatalytic degradation of CBZ.

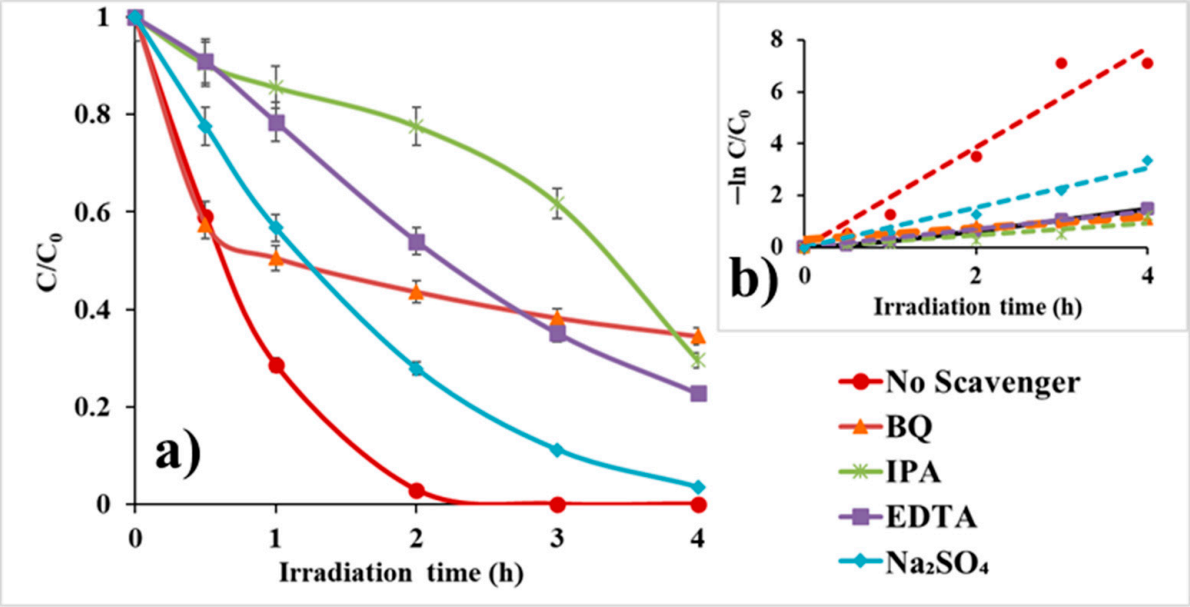

Figure 10. (**a**) Comparison of the photocatalytic CBZ degradation activities of the 0.05$CuWO_4$-TiO_2 photocatalyst in the presence of different scavengers, and (**b**) the apparent degradation rate constants (inset) (C_0 = 10 mg/L, catalyst dosage = 1.0 g/L, pH 8).

3.2.3. Effect of Hydrogen Peroxide (H_2O_2)

In order to understand the influence of hydrogen peroxide on the photocatalytic degradation process, 5 mM or 10 mM H_2O_2 were introduced into the reaction system. 0.05$CuWO_4$-TiO_2 showed no overall improvement in CBZ degradation after 4 h irradiation with neither 5 mM nor 10 mM H_2O_2 (Figure 11). The presence of an external oxidant like H_2O_2 may not have a positive effect due to the reason reported earlier that, at 365 nm UV light, H_2O_2 does have an extremely low absorption; hence, its generation of hydroxyl radical ($^{\bullet}OH$) via photolysis remains with little or no effect [54,55]. Some other likely reasons for the suppression of photocatalytic degradation of CBZ removal upon the addition of H_2O_2 may be the scavenging attitude of H_2O_2 towards hydroxyl radical ($^{\bullet}OH$) and perhaps the possible competition of 0.05$CuWO_4$-TiO_2 particle active sites such as surface contact reduction of CBZ with the catalyst that was needed for photocatalytic efficiency [54]. The 10 mM H_2O_2 showed stronger inhibition on CBZ degradation compared to lower 5 mM H_2O_2 concentration.

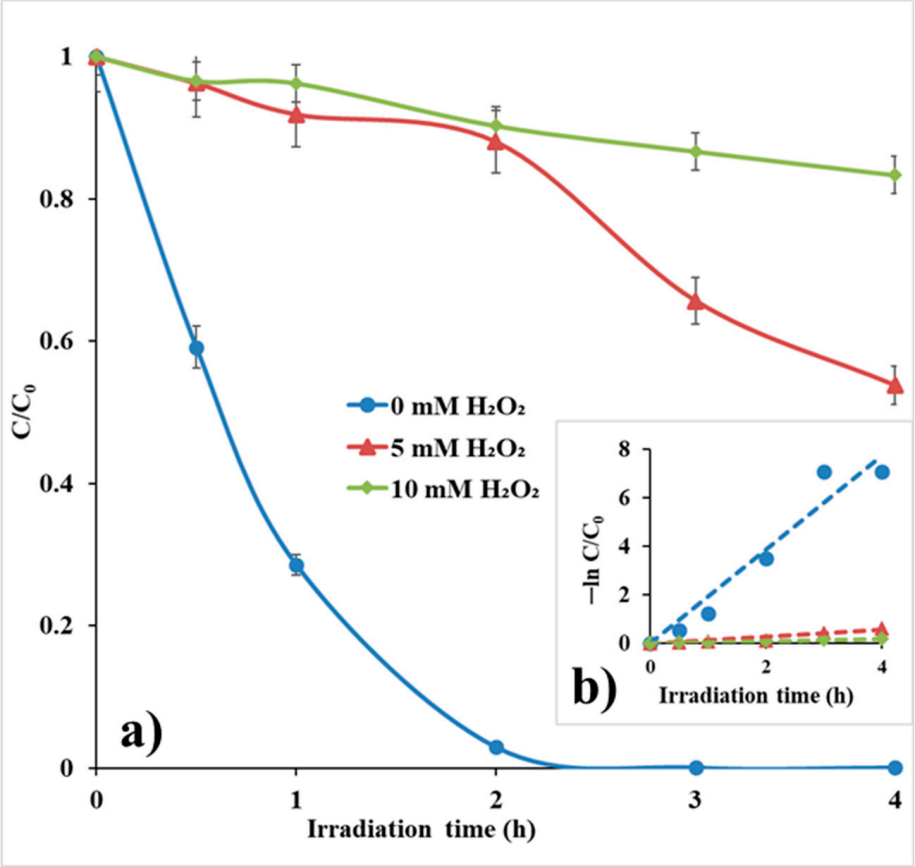

Figure 11. (**a**) Effect of H_2O_2 on photocatalytic degradation of CBZ (C_0 = 10 mg/L; catalyst dosage = 1.0 g/L, pH 8), and (**b**) the apparent degradation rate constant (inset).

3.2.4. Effect of Contaminant Ions and Humic Acid

Photocatalytic degradation of organic pollutants has been generally verified as not solely reliant on influences from factors such as catalyst dosage, contaminant load, and physico-chemical parameters like temperature, pH, light intensity, irradiation time, dissolved oxygen etc., but also on the water matrix environment contents in terms of inorganic ions and humic acid [48–50]. For this reason, some studies have suggested that inorganic ions and dissolved organic matter (DOM) usually present in the water matrix environment may in various ways play an inhibitory role against the photo efficiency of a catalyst either by scavenging present radicals, adsorption of other substrates onto the catalyst surface competitively or bringing about pH modifications of working suspensions [50]. In the present study, we investigated effects of some inorganic ions as well as humic acid as a surrogate DOM.

The effects of sodium inorganic anions: SO_4^{2-}, CO_3^{2-}, HCO_3^-, and NO_3^- (C_0 = 5 mg/L) were investigated in a single experimental test run for each ion (Figure 12). It can be observed that the CO_3^{2-} ion improved CBZ degradation, removing almost 100% after just 2 h and, therefore, can play a leading role in the degradation of some pollutants [52,53]. With HCO_3^-, an inhibitory effect towards the degradation rate of CBZ by the catalyst at 1 h irradiation time can be noticed. However, at 2 h irradiation, the introduction of this ion displayed lower inhibition towards CBZ degradation achieving over 90% degradation. From the observation made at 1 h irradiation time, HCO_3^- could act as a scavenger for hydroxyl radical inhibiting the degradation of CBZ initially. However, as $^{\bullet}CO_3^-$ radicals are formed with their scavenging properties, drastic CBZ removal at 2 h irradiation time was possible as can be further explained with Equations (4) and (5) highlighting more of the involved reaction mechanism:

$$HCO_3^- + {}^{\bullet}OH \rightarrow {}^{\bullet}CO_3^- + H_2O \quad (4)$$

$$CO_3^{2-} + {}^{\bullet}CO_3^{-} \rightarrow {}^{\bullet}CO_3^{-} + OH^{-} \quad (5)$$

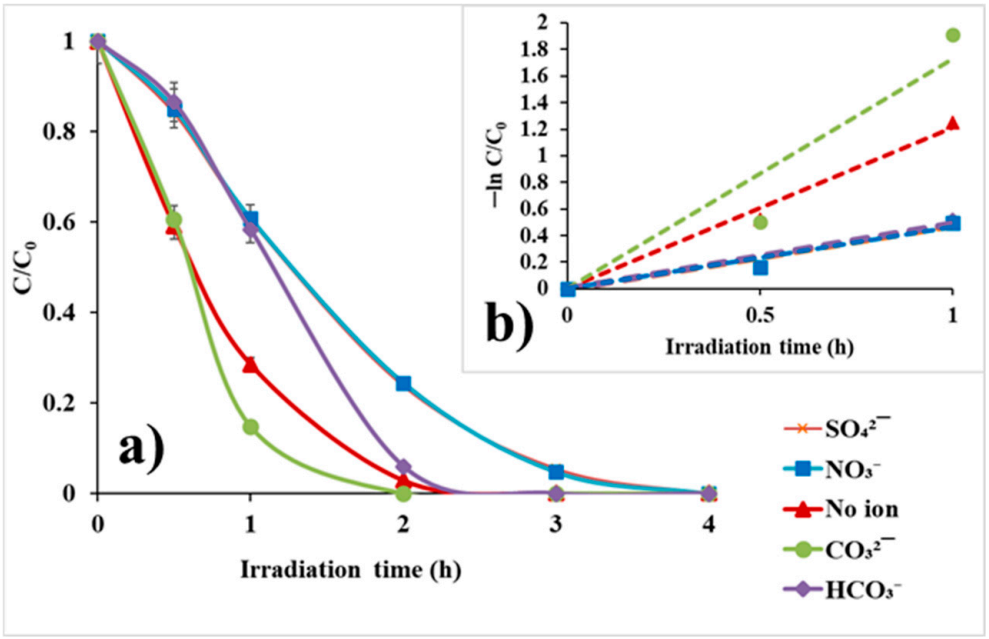

Figure 12. (**a**) Effect of anions on the photocatalytic degradation of CBZ (C_0 = 10 mg/L, catalyst dosage = 1.0 g/L, pH 8) in terms of singly added anions: SO_4^{2-}, CO_3^{2-}, HCO_3^{-}, NO_3^{-} (C_0 = 5 mg/L), and (**b**) the apparent degradation rate constant (inset).

This observation, on one hand, may contribute to the application of HCO_3^{-} and CO_3^{2-} ions as scavengers in testing for the participation of hydroxyl radicals ($^{\bullet}OH$) in aqueous based photoreaction processes and, on the other hand, might, under certain reaction concentration conditions, not interfere with pollutant degradation or even improve it [49]. The introduction of SO_4^{2-} and NO_3^{-} inhibited CBZ degradation with almost 20% of the CBZ still present after 2 h of irradiation. A possible reason for the low degradation rate of CBZ, noticed on the single addition of SO_4^{2-} as can be seen from Figure 12, may be attributed to the fact that SO_4^{2-} can adhere to TiO_2 based catalyst surface via Van der Waals forces and hydrogen bonds and may as such displace some surface hydroxyl group of TiO_2 via the ligand exchange mechanism (LEM) [49,55]. Apart from the high adsorption ability of SO_4^{2-} onto the surface of the catalyst due to its double charge, its high scavenging affinity towards $^{\bullet}OH$ might also have slowed down the CBZ degradation as compared to the rest [50]. The presence of NO_3^{-} exhibited similar inhibition effects on CBZ degradation and can be explained by the fact that NO_3^{-} could act as a scavenger for h^+ and $^{\bullet}OH$ (Equations (6) and (7)). However, the effectiveness of newly produced radicals is lower than the h^+ and $^{\bullet}OH$, which reduces the photocatalytic degradation of CBZ by the catalyst. These results are consistent with the previous reports on the effects of inorganic ions towards the degradation of CBZ [52,53].

$$NO_3^{-} + h_{vb}^{+} \rightarrow NO_3 \quad (6)$$

$$NO_3^{-} + {}^{\bullet}OH \rightarrow NO_3^{\bullet} + OH^{-} \quad (7)$$

Overall, the rate of photocatalytic oxidation of CBZ was not notably changed upon the single addition of these ions. This is an interesting result, but a more complex behavior is expected in natural aqueous systems.

Herein, to model the more complex water matrix rich in anionic species, the CBZ degradation test was carried out by combining these ions at various concentrations (Figure 13). In both solutions investigated, the degradation of CBZ was significantly reduced. These

results were consistent with previous results reporting photocatalytic deactivation of TiO_2 surface due to strong inhibition from inorganic ions as their presence counters colloidal stability, mass transfer increase, and reduces contact between pollutant and the photocatalyst [55].

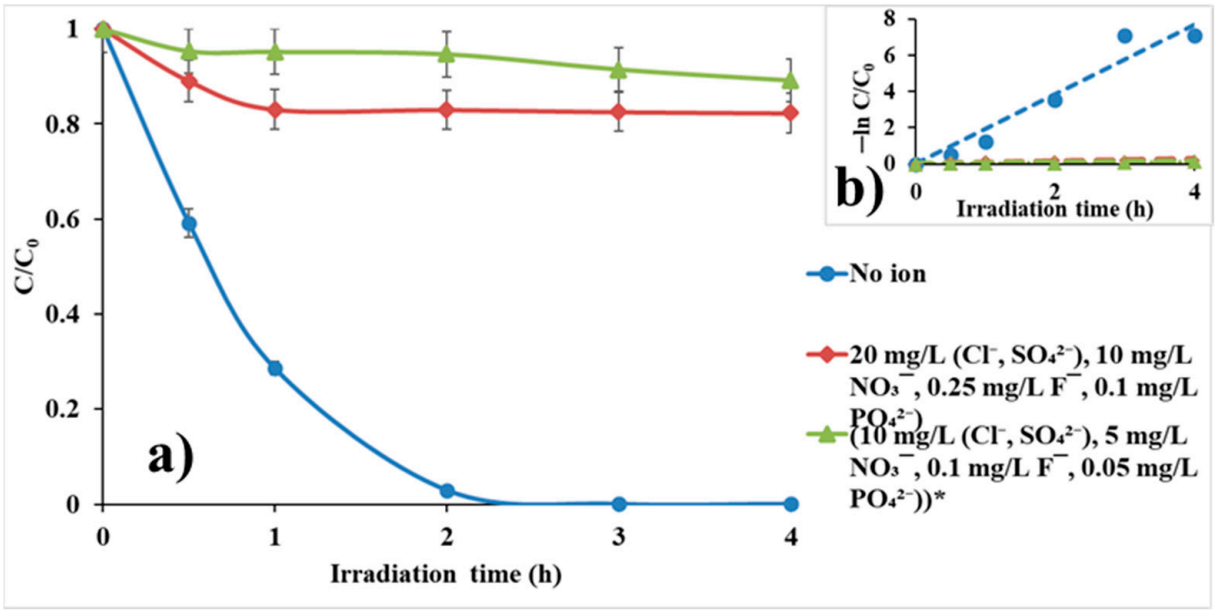

Figure 13. (**a**) Effect of mixed anions on the photocatalytic degradation of CBZ (C_0 = 10 mg/L, catalyst dosage = 1.0 g/L, pH 8]: (Cl^-, SO_4^{2-} (C_0 = 20 mg/L)), NO_3^- (C_0 = 10 mg/L), F^- (C_0 = 0.25 mg/L), and PO_4^{2-} (C_0 = 0.1 mg/L), and (Cl^-, SO_4^{2-} (C_0 = 10 mg/L), NO_3^- (C_0 = 5 mg/L), F^- (C_0 = 0.1 mg/L), and PO_4^{2-} (C_0 = 0.05 mg/L))*, and (**b**) the apparent degradation rate constants (inset). * lower concentration.

On the other hand, introduction of carbonate inorganic cationic species of Ca^{2+}, Na^+ (C_0 = 45 mg/L), Mg^{2+} (C_0 = 35 mg/L), and K^+ (C_0 = 20 mg/L) all in one test delivered a faster CBZ degradation with almost 100% removal after 2 h irradiation outperforming the investigated catalyst material 0.05$CuWO_4$-TiO_2 at this time with a degradation rate constant of ~2.68 h^{-1} (Figure 14, Table 2). At a lower concentration level of these ions: Ca^{2+}, Na^+ (C_0 = 20 mg/L), Mg^{2+} (C_0 = 15 mg/L), and K^+, Mg^{2+} (C_0 = 15 mg/L), the observed degradation rate constant was higher the first 30 min but soon decreased to 0.61 h^{-1} lower than when no ion was added. In the case of NH_4^+ at 1 mg/L concentration, a degradation rate constant of 0.86 h^{-1}, as compared to ~2.7 h^{-1} and ~1.32 h^{-1} degradation rate constants for multi- cation addition at respective higher and lower concentrations at 2 h irradiation, was observed (Figure 14, Table 2). However, at the tested concentration level of these ions, their effects were noticeable after 0.5 h, 1 h, and 2 h irradiation, as there was a delivery of a more concerted CBZ degradation effect. All in all, at 3 h irradiation, as can be seen from Figure 14, their effects were matched and similar towards CBZ degradation in comparison to no added ions. A literature report shows that some cations like calcium, magnesium, etc. have a negligible effect on the photodegradation of organic compounds and can be associated with the fact that these ions at their maximum oxidation states tend to show hampering effects towards degradation processes [52]. The inhibitory effect observed upon the addition of 1 mg/L NH_4^+ is remarkable, which, though hardly present in fresh water, exists normally in effluents of municipal wastewater treatment plants (MWWTP) following the mineralization of degraded organic compounds. Its inhibitory effect, as can be observed in Figure 14, is higher than the other cations and can be attributed also to surface adsorption active site accumulation instead of the pollutant [49,50].

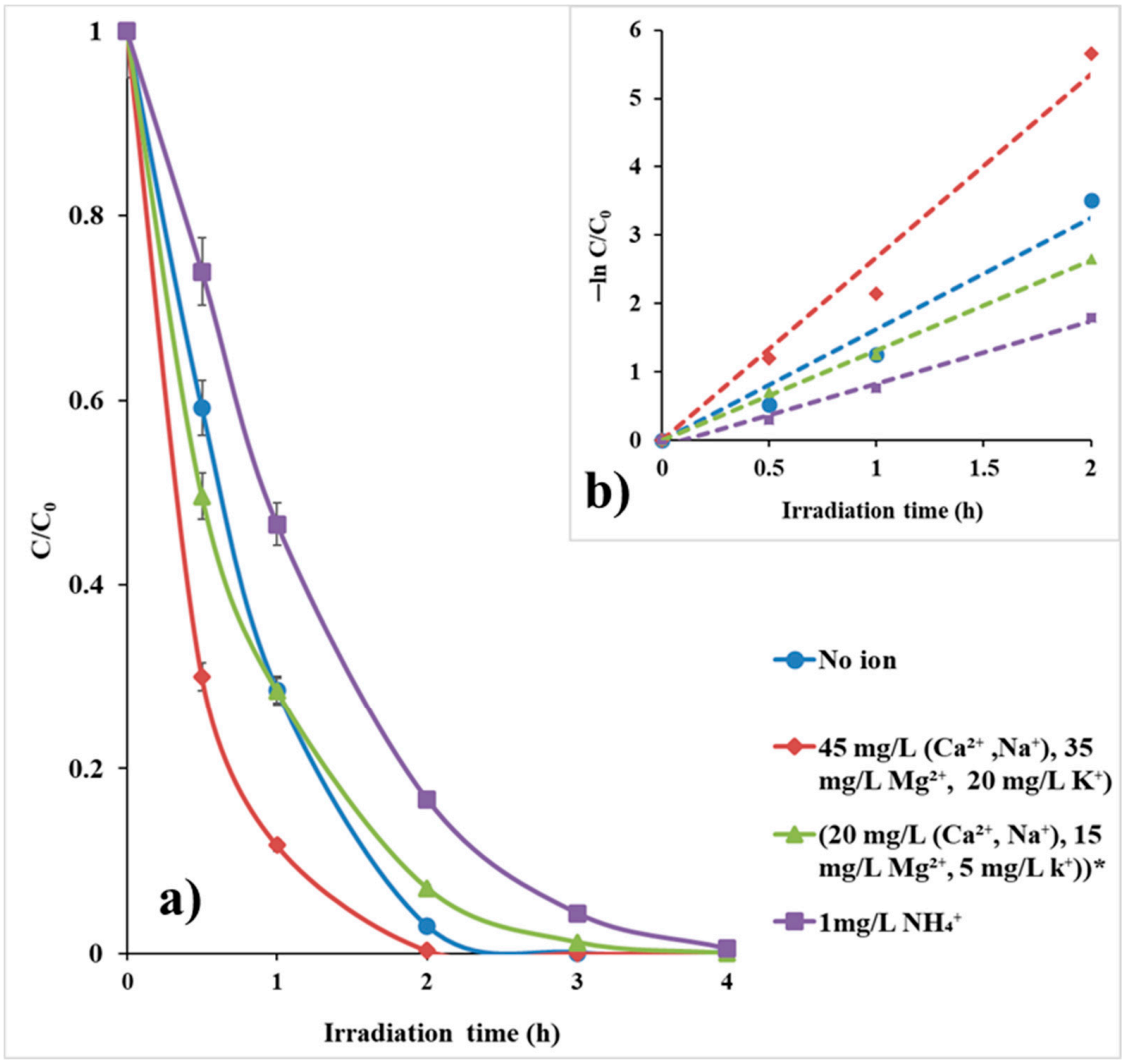

Figure 14. (**a**) Effect of mixed cations on the photocatalytic degradation of CBZ (C_0 = 10 mg/L; catalyst dosage = 1.0 g/L, pH 8): (Ca^{2+}, Na^+ (C_o = 45 mg/L)), Mg^{2+} (C_0 = 35 mg/L), and K^+ (C_0 = 20 mg/L), (Ca^{2+}, Na^+ (C_0 = 20 mg/L), Mg^{2+} (C_0 = 15 mg/L), K^+ (C_0 = 15 mg/L)*, and NH_4^+ (C_0 = 1 mg/L), and (**b**) the apparent degradation rate constants (inset). * lower concentration.

Figure 15 shows the effect of the humic acid (HA) on CBZ degradation. For this purpose, 5 and 10 mg/L HA were added to the reaction suspension to determine the effect of HA on the photocatalytic degradation of CBZ. The addition of HA has a negative effect on the degradation efficiency. The activity observed decreases as the concentration of HA increased. For instance, when the reaction suspension was spiked with 10 mg/L HA, CBZ degradation was reduced from almost 100 to about a little over 30 (%) at 4 h irradiation. Reduction efficiency of the catalyst on the addition of lower concentration of 5 mg/L HA was of a lower impact compared to the 10 mg/L HA concentration, though with a retarded degradation kinetics compared to 0 mg/L HA. The reduction in degradation can be attributed to: (i) the scavenging of photogenerated hydroxyl (•OH) radicals by HA as well its adsorbing onto TiO_2 that leads to the reduction of available active site for target substrate during photooxidation process [54], and (ii) reduced light penetration in the reaction medium [55].

Table 2 summarizes all the investigated photocatalytic parameters per photocatalytic material and their respective effect on CBZ degradation as identified by their estimated degradation rate constant K (h^{-1}) and their corresponding correlation factor (R^2) values.

An average value of triplicates is reported, and error bars have been indicated with standard deviation value of ±0.25 for all controlled photocatalytic activity parameters.

Table 2. Tested photocatalytic parameters at [C_0 = 10 mg/L CBZ], 1.0 g/L catalyst, corresponding degradation rate constant K (h^{-1}) and correlation coefficient (R^2) values.

Test	Degradation Rate Constant (h^{-1})	R^2
TiO_2 [n,¤]	0.8946	0.9993
$CuWO_4$ [n,¤]	0.0463	0.9877
$0.05CuWO_4$-TiO_2 [n,¤]	1.9243	0.9751
$1CuWO_4$-TiO_2 [n,¤]	0.5937	0.9701
$2CuWO_4$-TiO_2 [n,¤]	0.3053	0.9922
$3CuWO_4$-TiO_2 [n,¤]	0.0463	0.9877
$4CuWO_4$-TiO_2 [n,¤]	0.0463	0.9877
pH effects on $0.05CuWO_4$-TiO_2		
pH = 7.78	1.6287	0.9779
pH = 3	2.3303	0.9701
pH = 5	0.2592	0.9976
pH = 9	0.5702	0.9381
pH = 11	0.2592	0.9976
Scavenger effects on $0.05CuWO_4$-TiO_2 ¤		
No Scavenger	1.9243	0.9751
Benzoquinone (BQ)	0.3224	0.8952
Isopropyl alcohol (IPA)	0.2326	0.9006
Etheylenediamine tetracetic acid (EDTA)	0.3496	0.9915
Na_2SO_4	0.7664	0.9884
H_2O_2 effects on $0.05CuWO_4$-TiO_2 ¤		
0 mM H_2O_2	1.9243	0.9751
5 mM H_2O_2	0.2015	0.9215
10 mM H_2O_2	0.1957	0.8332
Ion effects on $0.05CuWO_4$-TiO_2: anions ¤,‡		
No ion	1.2112	0.9956
5 mg/L CO_3^{2-}	1.7302	0.9577
5 mg/L HCO_3^-	0.4618	0.9978
5 mg/L SO_4^{2-}	0.4618	0.9978
5 mg/L NO_3^-	0.4618	0.9978
Ion effects on $0.05CuWO_4$-TiO_2: anions ¤,#		
No ion	1.9243	0.9751
(20 mg/L (Cl^-, SO_4^{2-})), 10 mg/L NO_3^-, 0.25 mg/L F^-, 0.1 mg/L PO_4^{2-})	0.0321	0.6545
(10 mg/L (Cl^-, SO_4^{2-})), 5 mg/L NO_3^-, 0.1 mg/L F^-, 0.05 mg/L PO_4^{2-})) *	0.0221	0.6947
Ion effects on $0.05CuWO_4$-TiO_2: cations ¤,#		
No ion	1.6287	0.9793
(45 mg mg/L (Ca^{2+}, Na^+)), 35 mg/L Mg^{2+}), 20 mg/L K^+	2.6775	0.9897
(20 mg/L (Ca^{2+}, Na^+)), 15 mg/L Mg^{2+}, 5 mg/L K^+) *	1.316	0.9994
NH_4^+	0.8565	0.9921
Humic acid (HA) effects ¤		
0 mg/L HA	1.9243	0.9751
5 mg/L HA	0.7445	0.9864
10 mg/L HA	0.1389	0.8896

[n] Preliminary catalyst material selection, ¤ tested at $pH_{natural}$7.78, ‡ ions tested singly, # ions tested mixed, * tested ions of lower concentration.

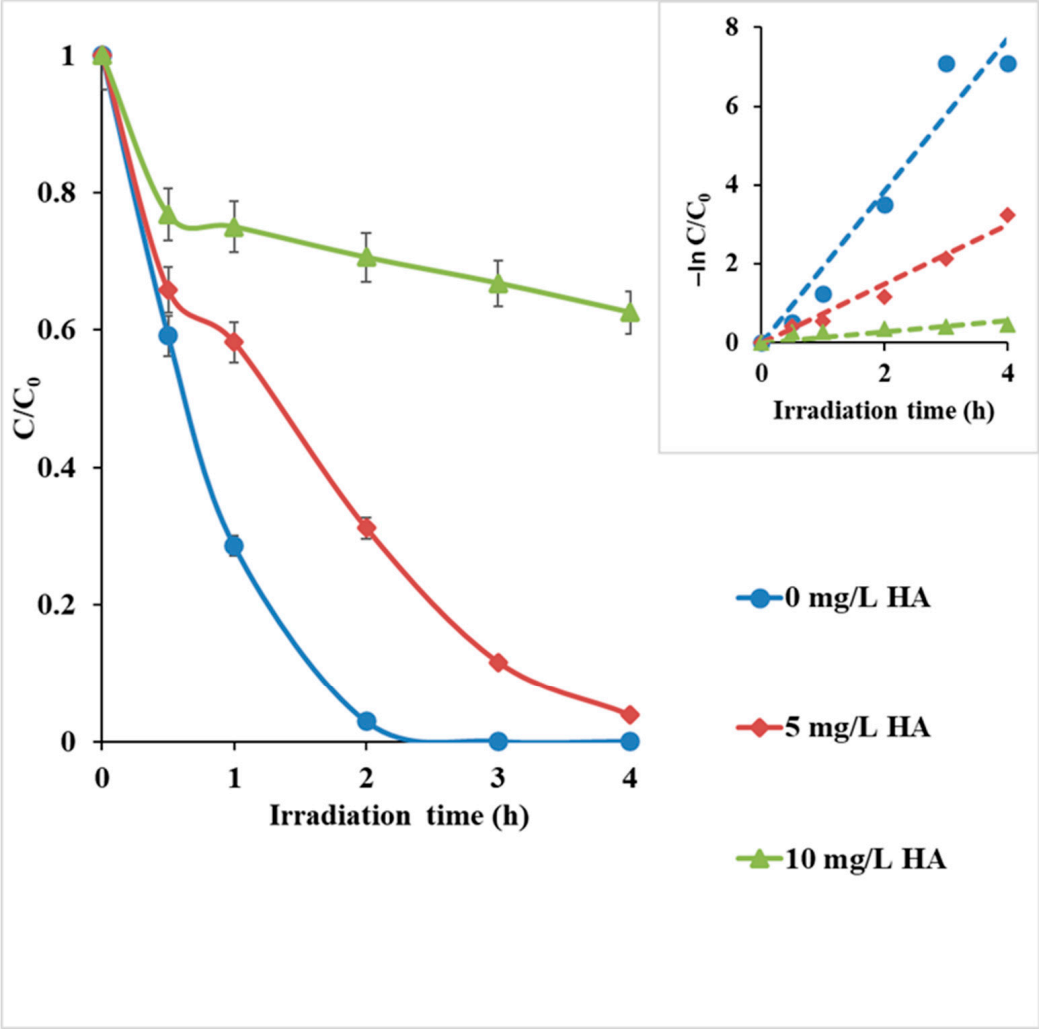

Figure 15. (**a**) Effect of humic acid (HA) on the photocatalytic degradation of CBZ (C_0 = 10 mg/L; catalyst dosage = 1.0 g/L, pH 8), and (**b**) the apparent degradation rate constants (inset).

3.3. Possible Mechanism of $CuWO_4$-TiO_2

After considering the scavenging experiments, the application of quenchers, and the discussion in Section 3.2.2, we have deduced that the probable pathway mechanism for CBZ degradation was a surface charge process driven by hydroxyl ($^{\bullet}OH$) radicals and superoxide anion ($O_2^{\bullet-}$) culminated by generation of valence band holes (h_{vb+}) and conduction band electrons (e_{cb-}) and their transfer accordingly. Such a pathway is supported by previous literature studies [9,17,19,48,56,57]. The photocatalytic activity of the 0.05$CuWO_4$-TiO_2 composite under UV light irradiation of 365 nm wavelength is illustrated in Scheme 1. Upon UV photon irradiation of the TiO_2 component of the composite material, there is excitation leading to the generation of valence band holes (h_{vb+}) and conduction band electrons (e_{cb-}) accompanied by possible redox reactions involving Cu^{2+}/Cu^{+} and or W^{+6}/W^{+5} redox systems. Due to favored energetics, the generated electrons of the TiO_2 conduction band drift into the conduction band of the $CuWO_4$ n-type semiconductor. During that time, electron-hole (e^{-}/h^{+}) charge recombination is suppressed as charges are more efficiently separated at the heterojunctions [56,57]. Consequently, more active species ($O_2^{\bullet-}$, $^{\bullet}OH$, h^{+}) are then becoming available to drive the photocatalytic reaction, which is therefore enhanced in comparison to either pure TiO_2 or $CuWO_4$ synthesized materials (Figure 7).

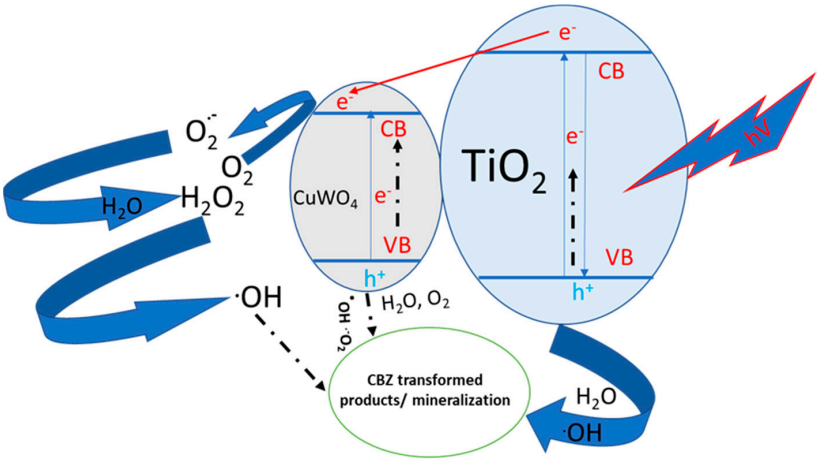

Scheme 1. Proposed surface charge process mechanism of $CuWO_4$-TiO_2 photocatalyst material.

3.4. Visible Light Photocatalyst Test

Photocatalytic activity of the synthesized 0.05$CuWO_4$-TiO_2 nanocomposite material was also tested under visible light employing the same light source already described in Section 2.4 of photocatalytic experiments, however, with an intensity of 2.3 mW/cm^2, and maximum wavelength centered at 450 nm of the emission spectrum 300–475 nm spectrum. As shown in Figure 16, it is observed that the 0.05$CuWO_4$-TiO_2 composite was not efficient towards CBZ degradation during 4 h irradiation time. However, with the addition of 5 mM H_2O_2, the composite material became active under visible light and achieved almost 60% CBZ degradation at 4 h irradiation time. Remarkably, upon the addition of H_2O_2 under the 365 nm irradiation in 5 and 10 (mM) concentrations, there was no outstanding photocatalytic activity of 0.05$CuWO_4$-TiO_2 material in terms of H_2O_2 enhancement (Figure 11). As earlier discussed in Section 3.2.3 under UV irradiation of 365 nm, H_2O_2 exhibits, among other properties, significantly low radiation absorption by photolysis in the suspension of some organic compounds [50–52]. In the test performed under 450 nm visible light (Figure 16), the addition of 5 mM H_2O_2 resulted in an improvement to the photocatalytic activity of the composite towards CBZ degradation. This may be attributed to the generation of hydroxyl (•OH) ions amongst other radical species in the reaction system despite the lack of activity of the majority of TiO_2 based materials under visible light [10].

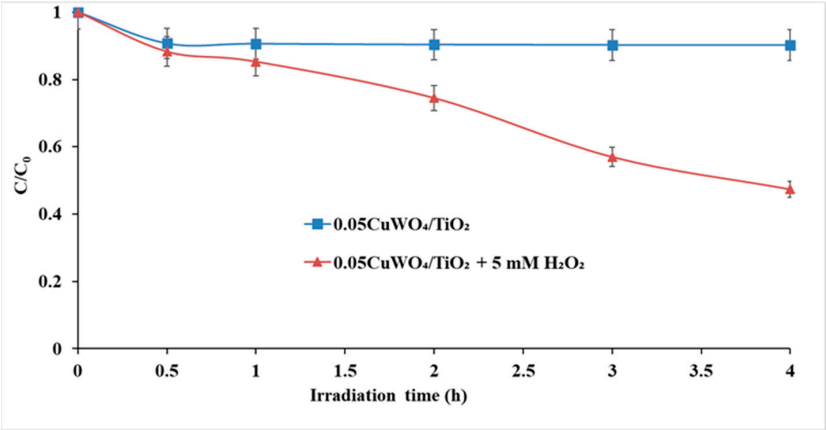

Figure 16. Photocatalytic degradation of CBZ by 0.05$CuWO_4$-TiO_2, (C_o = 10 mg/L, catalyst dosage = 1.0 g/L, pH 8) under 450 nm visible light in the presence of 5 Mm H_2O_2.

4. Conclusions

0.05$CuWO_4$-TiO_2 composite was synthesized by co-precipitation assisted hydrothermal method, homogenized in mixing under gentle mechanical agitation, and characterized for structural, morphological, and optical properties employing XRD, FTIR, BET, SEM, TEM, XPS, and UV-vis in DRS mode. Characterization data of 0.05$CuWO_4$-TiO_2 showed that anatase TiO_2 was the predominant phase but with a reduction in energy band gap (E_g) in comparison to the prepared unmodified TiO_2. The photocatalytic activity of the synthesized material was tested towards CBZ degradation under UV irradiation in various solution conditions. Preliminary testing was conducted under UV light irradiation for potential activity. 0.05$CuWO_4$-TiO_2 showed more effective CBZ degradation (almost 100%) under near visible light irradiation (365 nm) than pure TiO_2 after 2 h irradiation. Tests were performed investigating the effect of pH, H_2O_2, humic acid, and inorganic ions. Lower acidic pH 3 and moderately advanced pH 9 did not show significant inhibitory effect towards the degradation of CBZ. The $O_2^{\bullet -}$ and $^{\bullet}OH$ radicals were proposed as the responsible ROS for the degradation process. Tested cations in general improved the photocatalytic degradation of CBZ while their inorganic counterparts especially in multi-ion containing solutions decreased the photocatalytic degradation of CBZ. Finally, the 0.05$CuWO_4$-TiO_2 composite haven showed promising results also in the visible region deserves further study in the near future with more revelations on its potential application in wastewater treatment for the removal of CECs and especially of CBZ. Additionally, deeper insight into the charge transfer mechanism of the catalyst as a novel-Z scheme photocatalyst will be investigated.

Author Contributions: Conceptualization, C.B.A. and E.B.; Data curation, C.B.A., E.B. and V.N.S.; Formal analysis, C.B.A., I.A., E.B., T.K., M.H.B. and V.N.S.; Funding acquisition, I.A. and E.B.; Investigation, C.B.A. and M.H.B.; Methodology, C.B.A. and E.B.; Resources, C.B.A., E.B. and T.K.; Software, C.B.A., E.B. and T.K.; Supervision, I.A., E.B. and V.N.S.; Validation, C.B.A., E.B. and T.K.; Visualization, I.A., E.B., T.K. and V.N.S.; Writing—original draft, C.B.A.; Writing—review & editing, I.A., E.B., T.K., M.H.B. and V.N.S. All authors have read and agreed to the published version of the manuscript.

Funding: This research was funded by the EUROPEAN UNION'S HORIZON 2020 RESEARCH AND INNOVATION PROGRAMME under the MARIE SKLOWDOWSKA-CURIE Grant No: 765860 (AQUAlity).

Institutional Review Board Statement: Not applicable.

Informed Consent Statement: Not applicable.

Data Availability Statement: The Data presented in this study are available in [Enhanced Photocatalytic Activity of $CuWO_4$ Doped TiO_2 Towards Carbamazepine Removal Under UV Irradiation].

Conflicts of Interest: The authors declare no conflict of interest.

References

1. The 17 Goals. Available online: https://sustainabledevelopment.un.org/sdgs (accessed on 28 February 2020).
2. Anucha, C.B.; Altin, I.; Biyikglioglu, Z.; Bacaksiz, E.; Polat, I.; Stathopoulos, V.N. Synthesis, characterization, and photocatalytic evaluation of manganese (III) phthalocyanine sensitized $ZnWO_4$ ($ZnWO_4$MnPc) for bisphenol a degradation under UV irradiation. *Nanomaterials* **2020**, *10*, 2139. [CrossRef]
3. Jimenez-Holgado, C.; Crimatopoulos, C.; Stathopoulos, V.N.; Sakkas, V. Investigating the utility of fabric phase sorptive extraction and HPLC-UV-Vis/DAD to determine antidepressant drugs in environmental aqueous samples. *Separations* **2020**, *7*, 39. [CrossRef]
4. Rosenfeld, P.E.; Feng, L.G.H. Emerging contaminants. *Risks Haz. Wastes* **2011**, *1*, 215–222.
5. Jurado, A.; Sunez, E.V.; Ramirez, J.C.; Lopez de Alda, M.; Pujades, E.; Barcelo, D. Emerging organic contaminants in groundwater in Spain: A review of sources, recent occurrence and fate in a European context. *Sci. Total Environ.* **2012**, *440*, 82–94. [CrossRef]
6. Darabi, K.; Azhdarpoor, A.; Dehghani, M. Degradation of carbamazepine in aqueous solution using ozonation process removal of carbamazepine. *J. Health Sci. Surveill. Sys.* **2009**, *7*, 17–21.
7. NORMAN—Network of Reference Laboratories, Research Centres and Related Organizations for Monitoring of Emerging Environmental Substances. 2016. Available online: http://www.norman-network.net/ (accessed on 28 February 2020).
8. Susan, D.; Richardson, T.; Ternes, A. Water analysis: Emerging contaminants and current issues. *Anal. Chem.* **2014**, *86*, 2813–2848.

9. He, D.; Yang, Y.; Tang, J.; Zhou, K.; Chen, W.; Chen, Y.; Dong, Z. Synergistic effect of TiO_2-$CuWO_4$ on the photocatalytic degradation of atrazine. *Environ. Sci. Pollut. Res.* **2019**, *26*, 12359–12367. [CrossRef]
10. Janczarek, M.; Kowalska, E. On the origin of enhanced photocatalytic activity of copper-modified titania in the oxidative reaction systems. *Catalyst* **2017**, *7*, 317. [CrossRef]
11. Paola, A.D.; Palmisano, L.; Augugliaro, V. Photocatalytic behaviour of mixed WO_3/WS_2 powders. *Cat. Today* **2000**, *58*, 141–149. [CrossRef]
12. Lam, S.W.; Hermawan, M.; Coleman, H.M.; Fisher, K.; Amal, R. The role of copper (II) ions in the photocatalytic oxidation of 1,4-dioxane. *J. Mol. Catal. A* **2007**, *278*, 152–159. [CrossRef]
13. Wan, L.; Sheng, J.; Chen, H.; Xu, Y. Different recycle behavior of Cu^{2+} and Fe^{3+} ions for phenol photodegradation over TiO_2 and WO_3. *J. Haz. Mater.* **2013**, *262*, 114–120. [CrossRef] [PubMed]
14. Gawande, M.B.; Goswami, A.; Felpin, F.X.; Asefa, T.; Huang, X.; Silva, R.; Zou, X.; Zboril, R.; Varma, R.S. Cu and Cu-based nanoparticles: Synthesis and applications in catalysis. *Chem. Rev.* **2016**, *116*, 3722–3811. [CrossRef] [PubMed]
15. Reiche, H.; Dunn, W.W.; Bard, A.J. Heterogeneous photocatalytic and photosynthetic deposition of copper on TiO_2 and WO_3 powders. *J. Phys. Chem.* **1979**, *83*, 2248–2251. [CrossRef]
16. Lei, N.; Wang, L.; Zhu, H. Photocatalytic reductive degradation of polybrominated diphenyl ethers on CuO/TiO_2 nanocomposites: A mechanism based on the switching of photocatalytic reduction potential being controlled by the valence state of copper. *Appl. Catal. B* **2016**, *82*, 414–423. [CrossRef]
17. Xiong, X.; Chen, H.; Xu, Y. Improved photocatalytic activity of TiO_2 on the addition of $CuWO_4$. *J. Phys. Chem. C* **2015**, *119*, 5946–5953. [CrossRef]
18. Chen, H.; Xu, Y. Enhanced visible-light photoactivity of $CuWO_4$ through a surface-deposited CuO. *J. Phys. Chem. C* **2014**, *118*, 9982–9989. [CrossRef]
19. Vignesh, K.; Priyanka, R.; Hariharan, R.; Rajarajan, M.; Suganthi, A. Fabrication of CdS and $CuWO_4$ modified TiO_2 nanoparticles and its photocatalytic activity under visible light irradiation irradiation. *J. Ind. Eng. Chem.* **2014**, *20*, 435–443. [CrossRef]
20. Mavric, T.; Valant, M.; Foster, M.; Cowan, A.J.; Lavrencic, U.; Emin, S. Design of a highly photocatalytic active $ZnO/CuWO_4$ nanocomposite. *J. Colloid Int. Sci.* **2016**, *483*, 93–101. [CrossRef]
21. Siah, W.R.; Lintang, H.O.; Shamsuddin, M.; Yoshida, H.; Tuliati, L. Masking effect of copper oxides photodeposited on titanium dioxide: Exploring UV, visible, and solar light activity. *Catal. Sci. Technol.* **2016**, *6*, 5079–5087. [CrossRef]
22. Lan, X.; Wang, L.; Zhang, B.; Tian, B.; Zhan, J. Preparation of lanthanum and boron co-doped TiO_2 modified by sol-gel method and study of their photocatalytic activity. *Catal. Today* **2014**, *224*, 163–170. [CrossRef]
23. Mugundan, S.; Rajamannan, G.; Viruthagiri, N.; Shanmugam, R.; Gobi, P. Synthesis and characterization of undoped and cobalt-doped TiO_2 nanoparticles via sol-gel technique. *Appl. Nanosci.* **2015**, *5*, 449–456. [CrossRef]
24. Ahmed, M.A.; Khali, M.H.; Abdel-Ghany, H.A.; El-Gharbawy, S.A. Preparation and characterization of $CuWO_4$ nanoparticles. *J. Inorg. Nano Met. Chem.* **2020**. [CrossRef]
25. Lykaki, M.; Stefa, S.; Carabiniero, S.A.C.; Pandis, P.K.; Stathopoulos, V.N.; Kosolakis, M. Facet-dependent reactivity of Fe_2O_3/CeO_2 nanocomposites: Effects of ceria morphology on CO oxidation. *Catalysts* **2019**, *9*, 371. [CrossRef]
26. Trens, P.; Stathopoulos, V.N.; Hudson, M.J.; Pomonis, P. Synthesis and characterization of packed mesoporous tungstenosilicates: Application to the catalytic dehydrogenation of 2-propanol. *Appl. Catal. A* **2004**, *263*, 103–108. [CrossRef]
27. Bespalko, Y.; Kuznetsova, T.; Kriger, T.; Chesalov, Y.; Lapina, O.; Ischenko, A.; Larina, T.; Sadykov, V.; Stathopoulos, V. $La_2Zr_2O_7/LaAlO_3$ composite prepared by mixing precipitated precursors: Evolution of its structure under sintering. *Mater. Chem. Phys.* **2020**, *251*, 123093. [CrossRef]
28. Lima, A.E.B.; Costa, M.J.S.; Santos, R.S.; Batista, N.C.; Calvacante, L.C.; Longo, E.; Luz, G.E., Jr. Preparation of $CuWO_4$ porous films and their photoelectrochemical properties. *Electrochem. Acta* **2017**, *256*, 139–145. [CrossRef]
29. Turkten, N.; Cinar, Z.; Tomruk, A.; Bekbolet, M. Copper-doped TiO_2 photocatalysts: Application to drinking water by humic acid degradation. *Enviton. Sci. Pollut. Res.* **2019**, *26*, 36096–36106. [CrossRef] [PubMed]
30. Sajjad, A.K.L.; Shamaila, S.; Tian, B.; Chen, F.; Zhang, J. One step activation of WO_x/TiO_2 nanocomposites with enhanced photocatalytic activity. *Appl. Catal. B* **2009**, *91*, 397–405. [CrossRef]
31. Liu, G.; Han, C.; Pelaez, M.; Zhu, D.; Liao, S.; Likodimos, V.; Ioannidis, N.; Kontos, A.G.; Falaras, P.; Dunlop, P.S.M.; et al. Synthesis, characterization and photocatalytic evaluation of visible light activated C- doped TiO_2 nanoparticles. *Nanotechnology* **2012**, *23*, 294003. [CrossRef]
32. Praveen, P.; Viruthagiri, G.; Mugundan, S.; Shanmugam, N. Structural, optical and morphological analysis of pristine titanium di oxide nanoparticles- synthesized via sol-gel route. *Spectrochim. Acta Part A* **2014**, *117*, 622–629. [CrossRef]
33. Salmas, C.E.; Stathopoulos, V.N.; Promonis, P.J.; Androustsopoulos, G.P. Pore structure-chemical composition interactions of new high surface area manganese based mesoporous materials: Materials preparation, charcaterization, and catalytic activity. *Lagmuir* **2002**, *18*, 423–432. [CrossRef]
34. Pontes do Nascimento, N.M.; Machado de Lima, B.R.; Zamian, J.R.; Ferreira da Costa, C.E.; Santos do Nascimento, L.E.; Luque, R.; Narciso da Rocha Filho, G. Synthesis of mesoporous $Zn_{1-x}M_xAl_2O_4$ substituted Co^{2+} and Ni^{2+} ions and application in the photodegradation of rhodamine B. *Materials* **2020**, *13*, 2150. [CrossRef] [PubMed]
35. Ruggieri, F.; Di Camillo, D.; Maccarone, L.; Santucci, S.; Lozzi, L. Electrospun Cu-, W- and Fe-doped TiO_2 nanofibres for photocatalytic degradation of rhodamine 6G. *J. Nanopart. Res.* **2013**, *15*, 1982. [CrossRef]

36. Srivasan, M.; White, T. Degradation of methylene blue by three-dimensionally ordered macroporous titania. *Environ. Sci. Technol.* **2007**, *41*, 4405–4409. [CrossRef] [PubMed]
37. Hasan, M.d.R.; Abd Hamid, S.B.; Basirun, W.J.; Suhaimy, S.H.M.; Che Mat, A.N. A sol- gel derived, copper-doped, titanium dioxide- reduced graphene oxide nanocomposite electrode for the photocatalytic reduction of CO_2 to methanol and formic acid. *RSC Adv.* **2015**, *5*, 77803. [CrossRef]
38. Mathew, S.; Ganguly, P.; Rhatigan, S.; Kumaravel, V.; Byrne, C.; Hinder, S.J.; Bartlett, J.; Nolan, M.; Pillai, S.C. Cu doped TiO_2: Visible light assisted photocatalytic antimicrobial activity. *Appl. Sci.* **2018**, *8*, 2067. [CrossRef]
39. Bohra, D.; Smith, W.A. Improved charge separation via Fe doping of copper tungstate photoanodes. *Phys. Chem. Chem. Phys.* **2015**, *17*, 9857–9866. [CrossRef] [PubMed]
40. Gavade, N.L.; Babar, S.B.; Kadam, A.N.; Gophane, A.D.; Garadkar, K.M. Fabication of M@Cu_xO/ZnO (M = Ag, Au). Heterostructured nanocomposite with enhanced photocatalytic performance under sunlight. *Ind. Eng. Chem. Res.* **2017**, *56*, 14489–14501. [CrossRef]
41. Dashora, A.; Patel, N.; Kothari, D.; Ahuja, B.; Miotello, A. Formation of an intermediate band in the energy gap of TiO_2 by Cu–N-codoping: First principles study and experimental evidence. *Sol. Energy Mater. Sol. Cells* **2014**, *125*, 120–126. [CrossRef]
42. Hu, Q.; Huang, J.; Li, G.; Jiang, Y.; Lan, H.; Guo, W.; Cao, Y. Origin of the improved photocatalytic activity of Cu incorporated TiO_2 for hydrogen generation from water. *Appl. Surf. Sci.* **2016**, *382*, 170–177. [CrossRef]
43. Li, C.; Guo, B.; Peng, B.; Yue, C.; Diao, P. Copper tungstates ($CuWO_4$) nanoflakes coupled with cobalt phosphate (Co-Pi) for effective photoelectrochemical water splitting. *Int. J. Electrochem. Sci.* **2019**, *14*, 9017–9029. [CrossRef]
44. Tauc, J. Optical properties and electronic structure of amorphous Ge and Si. *Mater. Res. Bull.* **1968**, *3*, 37–46. [CrossRef]
45. Lalic, M.V.; Popovic, Z.S.; Vukajlovic, F.R. Ab initio study of electronic, magnetic, and optical properties of $CuWO_4$ tungstate. Compu. *Mat. Sci.* **2011**, *50*, 1179–1186.
46. Yourey, J.E.; Pyper, K.J.; Kurtz, J.B.; Bartlett, M.B. Chemical stability of $CuWO_4$ for photoelectrochemical water oxidation. *J. Phys. Chem. C* **2013**, *117*, 8708–8718. [CrossRef]
47. Mavengere, S.; Jung, S.-C.; Kim, J.-S. Visible light photocatalytic activity of $NaYF_4$: (Yb, Er)- CuO/TiO_2 composite. *Catalyst* **2018**, *8*, 521. [CrossRef]
48. Bang-De, L.; Xian-Qiang, X.; Yi-Ming, X. Improved photocatalytic activity for phenol degradation of rutile TiO_2 on the addition of $CuWO_4$ and possible mechanism. *Acta Phys. Chim. Sin.* **2016**, *32*, 1758–1764.
49. Gaya, U.I.; Abdullah, A.H. Heterogeneous photocatalytic degradation of organic contaminants over titanium dioxide: A review of fundamentals, progress and problems. *J. Photochem. Photobiol. C* **2008**, *9*, 1–12. [CrossRef]
50. Fang, G.; Zhou, D.; Dionysiou, D.D. Superoxide mediated production of hydroxyl radicals by magnetite nanoparticles: Demonstration in the degradation of 2- chlorobiphenyl. *J. Hazard. Mater.* **2013**, *250–251*, 68–75. [CrossRef]
51. Mori, A.; Kohno, M.; Masumizu, T.; Noda, Y.; Packer, L. Guanidino compounds generate reactive oxygen species. *Biochem. Mol. Biol. Int.* **1996**, *40*, 135–143. [CrossRef]
52. Canle, L.M.; Santaballa, J.A.; Vulliet, E. On the mechanism of TiO_2-photocatalyzed degradation of aniline derivatives. *J. Photochem. Photobiol. A* **2005**, *175*, 192–200. [CrossRef]
53. Velagraki, T.; Mantzavinos, D. Conversion of benzoic acid during TiO_2-mediated photocatalytic in water. *Chem. Eng. J.* **2008**, *140*, 15–21. [CrossRef]
54. Haroune, L.; Salaun, M.; Menard, A.; Legault, C.-Y.; Bellenger, J.-P. Photodegradation of carbamazepine and three derivatives using TiO_2 and ZnO: Effect of pH, ionic strength, and natural organic matter. *Sci. Total Environ.* **2014**, *475*, 16–22. [CrossRef] [PubMed]
55. Ma, H.-Y.; Zhao, L.; Guo, L.-H.; Zhang, H.; Chen, F.-J.; Yu, W.-C. Roles of Reactive Oxygen Species (ROS) in the photocatalytic degradation of pentachlorophenol and its main toxic intermediates by TiO_2/UV. *J. Hazard. Mater.* **2019**, *369*, 719–726. [CrossRef] [PubMed]
56. Ali, S.; Lee, J.; Kim, H.; Hwang, Y.; Razzaq, A.; Jung, J.-W.; Cho, C.-H.; In, S.-I. Sustained, photocatalytic CO_2 reduction to CH_4 in a continuous flow reactor by earth-abundant materials: Reduced titania-Cu_2O Z-scheme heterostructures. *Appl. Catal. B* **2020**, *279*, 119344. [CrossRef]
57. Kim, H.R.; Razzaq, A.; Grimes, G.A.; In, S.-I. Heterojunction p-n-p Cu_2O/S-TiO_2/CuO: Synthesis and application to photocatalytic conversion of CO_2 to methane. *J. CO_2 Util.* **2017**, *20*, 91–96. [CrossRef]